Stratigraphic and Microfossil Evidence of Repeated Late Holocene Tsunami Inundation at Sitkalidak Island, Alaska

Alexa Brianne Prater

Thesis submitted to the faculty of the Virginia Polytechnic Institute and State University in partial fulfillment of the requirements for the degree of

Master of Science
In
Geosciences

Cristina Dura
James Spotila
Brian Romans

September 10th, 2021
Blacksburg, Virginia

Keywords: (Alaska, paleoseismology, earthquakes, tsunamis, diatoms)

Stratigraphic and Microfossil Evidence of Repeated Late Holocene Tsunami Inundation at Sitkalidak Island, Alaska

Alexa Brianne Prater

ABSTRACT

Seismic hazard models for Alaska require estimates of the size and frequency of prehistoric megathrust earthquakes. However, observations that place limits on the size of subduction paleoearthquakes along the Alaska-Aleutian subduction zone are scarce. To help place bounds on the along-strike extent of prehistoric Alaska-Aleutian subduction ruptures, we present stratigraphic and microfossil evidence of repeated tsunami inundation over the last ~400 years at Sitkalidak Island, located 0.5 km off the coast of south-central Kodiak Island. Peat cores collected from an estuary in southern Sitkalidak Island reveal three anomalous, laterally continuous sand beds with sharp upper and lower contacts preserved within a coastal peat sequence. The microfossil and lithostratigraphic characteristics of the sand beds, including the presence of anomalous marine planktonic diatoms, high fragmentation of diatoms, and upward fining sand sequences, indicate high-energy marine incursions consistent with tsunami inundation. Radiocarbon dating constrains the deposition of the sand beds to AD 1964, AD 1788, and ~400 cal yr B.P. The peat core stratigraphy and dates are consistent with tidal wetland stratigraphic records observed at sites ~90 km to the west at Sitkinak Island, and ~80 km to the east at Middle Bay, Kodiak Island. Diatom results from Sitkalidak Island suggest decimeter-scale subsidence during the deposition of the AD 1964 and AD 1788 sand bed. Deformation concurrent with the 1964 and 1788 ruptures along with the presence of a sand bed associated with the ~400 cal yr BP rupture at Sitkalidak help better define the western and eastern rupture limits, and thus the permissible maximum magnitudes, of past Alaska-Aleutian subduction zone ruptures.

Stratigraphic and Microfossil Evidence of Repeated Late Holocene Tsunami Inundation at Sitkalidak Island, Alaska

Alexa Brianne Prater

GENERAL AUDIENCE ABSTRACT

The Alaska-Aleutian subduction zone experiences frequent great earthquakes over magnitude 8 which often produce far-reaching tsunamis. Seismic hazard models that help coastal communities predict and prepare for future hazards require estimates of the size and frequency of prehistoric earthquakes. Data for prehistoric earthquake events in the western region of the subduction zone is scarce. To help address the lack of prehistoric data and understand the rupture path and magnitude of past Alaska-Aleutian earthquakes, we present stratigraphic and microfossil evidence of repeated tsunami inundation over the last ~400 years at Sitkalidak Island, located 0.5 km off the coast of south-central Kodiak Island, Alaska. Sediment cores collected from a marsh in southern Sitkalidak Island record three laterally continuous sand beds with sharp stratigraphic contacts preserved within a coastal peat. Diatom microfossil and grain-size characteristics of the sand beds indicate high-energy marine incursions consistent with chaotic tsunami inundation. Radiocarbon dating places the age of sand bed deposition to AD 1964, AD 1788, and ~400 cal yr B.P. The sediment core stratigraphy and dating correlates well with sites investigated ~90 km to the west and ~80 km to the east. Diatom results from Sitkalidak Island point to small, decimeter scale coseismic subsidence during the deposition of the AD 1964 and AD 1788 sand beds. Land-level change concurrent with the 1964 and 1788 earthquakes along with the presence of a sand bed associated with the ~ 400 cal yr B.P. earthquake found at Sitkalidak Island help better define the earthquake rupture limits and maximum magnitudes of past Alaska-Aleutian subduction zone earthquakes.

ACKNOWLEDGEMENTS

I would like to first thank my advisor Dr. Tina Dura for her unending support, direction, and advice throughout my time pursuing my Master's degree. I have learned much about being a professional researcher and woman in geosciences from you, and greatly value the time I have had with you as an advisor, mentor, and friend. You have helped me gain confidence in myself as a geologist and person. Thank you for introducing me to the fascinating world of paleoseismology and diatom microfossils!

To my committee members Jim Spotila and Brian Romans, thank you for being so incredibly supportive over the past two years in which my progress was hindered by the pandemic and all the resulting challenges. Your feedback and questions helped me better understand the bigger picture of my research, and see my project through new angles.

Also, much thanks to my incredibly supportive and helpful lab mates, Jessica DePaolis and David Bruce. Our many talks helped orient my direction, destress my mind, and ultimately kept me sane throughout the past two years. Thank you for being incredible friends and colleagues.

Lastly, thank you to my loving and supportive parents and husband who never once doubted my capabilities and always believed in my ability to succeed. This achievement could not have been possible without your unconditional love and support.

TABLE OF CONTENTS

1. INTRODUCTION

Coastal geologic studies that combine coastal geomorphology, paleoseismology, micropaleontology, geophysics, and sea-level research methods have proven to be an effective approach to reconstructing the earthquake and tsunami history of a subduction zone over millennial timescales (Atwater, 1987; Sawai, 2004; Stein & Okal, 2007; Nelson et al., 2008). The importance of coastal geologic records of past earthquakes and tsunamis was underscored by the devastating effects of both the 2011 Tohoku and 2004 Indian Ocean tsunamis, which can be partially attributed to an incomplete understanding of prehistoric earthquakes occurring on the Sunda and Japan subduction zones, respectively (Sawai, 2004; Rhodes et al., 2006; Dura, Engelhart, et al., 2016). Since those events, geologic studies on coastlines bordering the Sunda and Japan subduction zones have uncovered >500-year-old tsunami deposits, indicating a history of previous large tsunami inundation in these locations, and expanding the knowledge of great earthquake recurrence intervals (Jankaew et al., 2008; Stein & Okal, 2007, 2011). Such geologic discoveries benefit the improvement of seismic and tsunami hazard maps that help vulnerable coastlines prepare for future disasters (Mueller et al., 2015).

In North America, an extraordinary series of great earthquakes (>M_w8) and associated tsunamis characterize the Alaska-Aleutian subduction zone throughout the 20th century. However, geologic observations that place limits on the size of prehistoric earthquakes are mainly focused along the eastern portion of the subduction zone (Shennan et al., 1999; Shennan & Hamilton, 2006; Shennan et al., 2009; Shennan, et al., 2014) and are scarce in the western Kodiak Island region near the western extent of the AD 1964 M_w9.2 rupture (Briggs et al. 2014; Shennan et al. 2014; Nelson et al. 2015). The lack of field data in this region leaves questions about the permissible

bounds of prehistoric earthquakes and how those bounds should be incorporated into seismic hazard maps (Briggs et al., 2014; Shennan, Barlow, et al., 2014; Shennan et al., 2018). One outstanding question in the region is whether the boundary between the AD 1964 and the AD 1938 M_w8.2 ruptures is a long-lived rupture barrier (Wesson et al., 2007). Coastal geologic and seismic reflection studies (von Huene et al., 2016) completed in the last decade in the western Kodiak Island region have begun to call into question the persistence of the boundary (Figure 1a), showing that an earthquake in 1788 (M_w8-9) and two additional ruptures may have crossed the proposed rupture barrier (Briggs et al., 2014). The potential for variation in rupture boundaries between earthquakes illustrates the importance of geologic studies in a region that has the potential to generate large tsunamis directed at far-field sites including Hawaii and the western coast of the United States (Shennan et al., 2009; Ross et al., 2013; von Huene et al., 2016).

Coastal geologic datasets of earthquakes and tsunamis hinge upon the earthquake deformation cycle. The earthquake deformation cycle is characterized by meter to decimeter-scale interseismic, coseismic, and postseismic deformation that can be recorded within coastal sediments as a series of relative sea-level (RSL) changes (Nelson et al., 1996; Dura et al., 2015; Garrett et al., 2015). Sudden coseismic uplift or subsidence of the coast is represented by sharp lithologic contacts and abrupt environmental change while gradual deformation during the postseismic and interseismic periods is represented by gradual lithologic contacts and slow environmental change (Dura, Engelhart, et al., 2016). In some locations, widespread sand beds deposited by tsunamis accompanying great earthquakes can be linked with lithologic evidence of sudden RSL change associated with coseismic deformation (Shennan et al., 1999; Sawai, 2004; Hamilton & Shennan, 2005a). Earthquakes and tsunami histories that extend through multiple earthquake cycles have been developed using stratigraphic evidence from subduction zones around the world, including

Chile (Garrett et al., 2015; Cisternas et al., 2017; Dura et al., 2017), Japan (Sawai, 2004; Sawai et al., 2012), the Indian Ocean (Jankaew et al., 2008), the Pacific Northwest of the United States(Witter et al., 2003; Nelson et al., 2020), and Alaska (Hamilton & Shennan, 2005b; Briggs et al., 2014; Witter et al., 2014; Nelson et al., 2015).

Coastal geologic studies employ a variety of proxies to characterize environmental changes associated with the earthquake deformation cycle. Such proxies include grain size, geochemistry, and microfossils (e.g., foraminifera, pollen, and diatoms). Because of their sensitivity and quick response to changes in environmental variables such as PH, tidal exposure, salinity, and substrate, diatoms in particular have proven to be a valuable tool in discerning tectonically driven RSL change and tsunami inundation (Figure 2). Diatoms have been utilized in coastal geologic reconstructions of earthquakes and tsunamis at subduction zones worldwide (Hawkes et al., 2010; Wang et al., 2013; Dura, Hemphill-Haley, et al., 2016; Horton et al., 2017), and have been especially effective along the Alaska-Aleutian subduction zone (Zong et al., 2003; Watcham et al., 2013; Hamilton et al., 2005).

Here, we reconstruct the history of coseismic deformation and tsunami inundation on Sitkalidak Island (Figure 1b), located within the proposed overlap of the 1788 and 1964 ruptures. We apply stratigraphic, sedimentological, and diatom methods to a sediment core taken from Ocean Bay marsh (Figure 1c), Sitkalidak Island, and document evidence of tsunami inundation and potential coseismic subsidence associated with earthquakes in AD 1964, AD 1788, and ~400 cal yr B.P. Our new earthquake and tsunami reconstruction from Sitkalidak Island helps better define the trench-parallel rupture extent and trench-perpendicular zone of deformation during past earthquakes in the western Kodiak Island region.

2. TECTONIC AND COASTAL SETTING

2.1 Seismic and Tsunami History in South-Central Alaska

The Alaska-Aleutian subduction zone marks the plate boundary between the subducting Pacific Plate and the continental North American Plate, extending ~4000 km from the eastern edge of the Gulf of Alaska to the Kamchatka Peninsula. The central region of the subduction zone, encompassing the Kodiak and Semidi segments, converges orthogonally at 57-64 mm/yr at a shallow dipping angle of <10° (Figure 1a; Carver & Plafker, 2013; von Huene et al., 2016). Geodetic research indicates that the Kodiak and Semidi segments are >90% locked and accumulating strain (Fournier & Freymueller, 2007). The Kodiak-Bowie seamount chain to the east (56°N) and the Aja Fracture Zone and Patton Murray seamount chain to the west (55°N) create plate boundary asperities that border the central Kodiak segment and may create barriers that limit rupture length (Briggs et al., 2014; von Huene et al., 2016).

Historical and prehistoric earthquakes have defined the general pattern of deformation at coastal sites bordering the Kodiak segment of the subduction zone (Plafker, 1965; Shennan, Barlow, et al., 2014). At locations more than ~120 km from the subduction zone, the general pattern of coastal deformation is gradual interseismic uplift lasting centuries to millennia followed by sudden, instantaneous coseismic subsidence (Thatcher, 1984; Hamilton & Shennan, 2005b; Wright, 2016). In coastal sedimentary sequences, coseismic subsidence is often represented by a peat-silt couplet: an organic rich peat formed in an upland or high-marsh environment abruptly overlain by minerogenic, fine-grained lower-intertidal sediment (Figure 2; Hemphill-Haley, 1996; Garrett et al., 2015). At locations closer to the subduction zone (~120 to ~90 km), the earthquake deformation cycle is characterized by gradual interseismic subsidence lasting centuries to millennia followed by sudden, instantaneous coseismic uplift. In coastal sedimentary sequences,

coseismic uplift is often represented by a silt-peat couplet: minerogenic, fine-grained lower-intertidal sediment abruptly overlain by an organic-rich peat formed in an upland or high marsh environment. The addition of an anomalous sand bed lying on the peat-silt or silt-peat contact is commonly interpreted to be the result of tsunami inundation occurring at the same time or shortly after coseismic deformation (Nelson et al., 1996; Dawson & Stewart, 2007; Sawai et al., 2012).

The earthquake deformation cycle in the western Kodiak Island region and west into the Semidi segment has proven to be complex. Recent work documenting prehistoric earthquakes in the western Kodiak Island region has shown that depending on the distribution of slip, the proximity of coastal sites to the edges of ruptures, and upper plate faulting, both coseismic uplift and/or subsidence can be recorded in the stratigraphy of one location (Briggs et al., 2014). Mixed records of coseismic uplift and subsidence at one coastal site have also been described in Chile (Dura et al., 2017), notably at locations where ruptures overlap or terminate.

The three most recent large earthquakes to affect the Kodiak and Semidi segments occurred in AD 1964, AD 1788, and ~400 cal yr B.P (Figure 1a). The presence or absence of geologic evidence of the three earthquakes in the coastal geologic record at sites in the eastern (e.g., Shuyak, Middle Bay, Kalsin Bay, Anton Larson Bay; (Shennan et al., 2014, 2018) and western (e.g., Chirikof, Sitkinak, Old Harbor) Kodiak Island regions illustrates the complexity of ruptures along the Kodiak and Semidi segments (Figure 1a, 3; Briggs et al., 2014; Nelson et al., 2015; Janigian, 2018). The multi-segment (i.e., Kodiak, Kenai, Prince William Sound segments) M9.2 Alaskan earthquake of 1964 ruptured nearly ~950 kilometers of the subduction zone and caused far-field tsunami inundation of up to ~9 m at Kodiak, Alaska (Kachadoorian & Plafker, 1967; Eckel, 1970). The earthquake caused widespread uplift and subsidence from Prince William Sound to Sitkinak Island, but slip did not reach far enough west to affect Chirikof Island. In eastern Kodiak (i.e.,

Shuyak, Middle Bay, Kalsin Bay, Anton Larson Bay), Shennan et al. (2014, 2018) document geologic evidence of coastal subsidence and tsunami sand deposition for the 1964 earthquake, consistent with observations of marsh submergence in eastern Kodiak (Plafker, 1969). At Sitkinak Island, Briggs et al. (2014) describe geologic evidence for subsidence and tsunami inundation along the southern coast, while a historical account reports <1 m of uplift on the northern coast in 1964. The variability in surface deformation across the island can be explained by the termination of rupture at or near Sitkinak that produced a subsidence trough, which wrapped around the zone of uplift (Briggs, 2006). At Old Harbor, Engelhart et al. (2018) and Janigian et al. (2018) document a thick (17 cm) tsunami deposit but no land-level change evidence for the 1964 earthquake. This geologic observation is in contrast with observations of up to ~0.9 m of subsidence near Old Harbor (Plafker & Kachadoorian, 1966; Kachadoorian & Plafker, 1967).

Stratigraphic evidence of a tsunamigenic earthquake occurring in AD 1788 has been reported from sites in eastern (i.e., Shuyak, Middle Bay, Kalsin; Shennan et al., (2014, 2018) and western Kodiak Island (Old Harbor, Sitkinak, Chirikof), corroborating sparse historical accounts by Russian settlers reporting ground shaking and 3-10 m of tsunami inundation during the summer of AD 1788 at Three Saints Bay, Kodiak Island (Soloviev, 1990; Briggs et al., 2014; Nelson et al., 2015; Janigian, 2018). The coastal geologic evidence and historical accounts of tsunami inundation and coastal deformation in 1788 suggest a rupture extent encompassing at least the Kodiak and part of the Semidi segment (Figure 3). However, despite historical accounts suggesting a high tsunami in 1788 event near the Shumagin Islands, no evidence of the event has been found on Sanak, Simeonof, or Unga Islands, leaving questions about the western extent of the rupture (Witter et al., 2014; Engelhart et al., 2018).

At sites in the eastern and western Kodiak Island regions, coastal geologic studies have documented stratigraphic and microfossil evidence of a large earthquake and associated tsunami in ~400 cal yr BP (Carver et al., 1992; Gilpin, 1995; Shennan, Barlow, et al., 2014). On Shuyak Island, Shennan et al. (2018) describe stratigraphic and microfossil evidence for possible subsidence without a tsunami, although more correlations are needed to confirm. On Sitkinak Island, Briggs et al., (2014) describe stratigraphic and diatom evidence for uplift and tsunami inundation occurring between 520-300 cal yr BP, inferred to be the same ~400 cal yr BP event documented in eastern Kodiak Island (i.e., Shuyak). Further west, on Chirikof Island, one documented tsunami deposit dated to 510-317 cal yr B.P was inferred to be a separate event, suggesting Chirikof lies outside the rupture patch for the 400 cal yr B.P. earthquake (Nelson et al., 2015).

2.2 Sitkalidak Island

In this study we target Sitkalidak Island, Alaska which lies along a transect of coastal geologic sites spanning the eastern and western Kodiak regions (Figure 1a, b). The location of the island allows us to address outstanding questions about both the trench-perpendicular (axis of deformation) and trench-parallel (rupture limit) slip extent during past earthquakes. Sitkalidak Island is separated from the southern shore of Kodiak Island by the Sitkalidak Strait and lies ~120 km northwest of the Alaska-Aleutian subduction zone. Tertiary age sedimentary and volcanic rock underlies the uninhabited island, and its topography consists of low elevation freshwater and saline marshes bordered by high-relief mountains.

The majority of Sitkalidak Island experienced coseismic subsidence of up to 2.5 m and tsunami inundation during the AD 1964 earthquake (Carver & Plafker, 2013). An account by a local resident just after the AD 1964 earthquake describes a zone of <1 m uplift of the extreme

southeastern coast Sitkalidak Island (Plafker, 1969). Current GPS station measurements at Sitkinak Island (~80 km SW of Sitkalidak) and Old Harbor (~15 km N of Sitkalidak) show interseismic subsidence of ~7 mm/yr and uplift of ~4 mm/yr, respectively. This places southern Sitkalidak Island near the hinge line between interseismic uplift and subsidence, consistent with the observations of Plafker, (1969) that placed southern Sitkalidak Island near the 0-m contour (i.e., hinge line) of the 1964 rupture. The location of Sitkalidak between the subsiding Sitkinak Island and uplifting Old Harbor is a prime position to use coastal geologic methods to test the observations of deformation made following the 1964 earthquake (Plafker & Kachadoorian, 1966; Kachadoorian & Plafker, 1967; Eckel, 1970), and apply the same methods to older events in the stratigraphic record to reconstruct potential past deformation of the island.

3. APPROACH AND METHODOLOGY

3.1 Site Reconnaissance and Sampling

We targeted Ocean Bay marsh in southern Sitkalidak Island for our coastal geologic study. Ocean Bay marsh borders south-facing Ocean Bay and lies between 1-2 m above mean tide level (MTL). The marsh is intersected by tidal channels and is dominated by the salt marsh plants *Carex* sp and *Triglochin* sp. To reconstruct the earthquake and tsunami history of Ocean Bay marsh, we described ~74 exposures, soil pits, and sediment cores to a depth of 1-2 m. Soil pits and gouge core samples were completed in coast perpendicular and coast parallel transects to discern the lateral and landward extent of past environmental change and tsunami sediment deposition. In the field, detailed descriptions of the stratigraphy including sharpness of upper and lower contacts, grain size, depth, and estimates of the proportion of organics, clay, silt, and sand were completed using the Troels-Smith method for the description of organic-rich sediment (Troels-Smith, 1955). Cores representative of site stratigraphy were identified in the field and sampled with both Russian and gouge corers for laboratory analyses. Coordinates and elevations of each sampling site were recorded using a differential GPS and then extrapolated to a tidal datum measured using a tide gauge to determine site elevations relative to local mean tide level (MTL).

This paper focuses on the detailed analysis of sediment core OBL.15.W14, which was collected from the bank of an estuarine tidal channel (57.09083°, -153.20094°) ~570 m from the surf line and inland of the beach berm lying parallel to Ocean Bay. The coring location is 0.5-1 m lower in elevation than the surrounding marsh and was noted in the field as potentially containing lithologic evidence of both land-level change and tsunami inundation. Overlapping 50-cm-long, 5-cm-diameter core lengths were collected at location OBL.15.W14 (hereafter referred to as W14) down to ~1 m depth.

3.2 Sediment Preparation and Grain Size Analysis

In order to characterize the grain size distributions throughout core W14 and identify anomalously course sediment potentially deposited by tsunamis, we conducted high-resolution grain size analysis. We subsampled the core at 1-cm intervals near lithologic contacts of interest. Each sample was treated with 30% concentrated hydrogen peroxide (H_2O_2) to dissolve organic matter. Due to the high percentage of organic matter within core W14, the digestion processes began with two weeks of slow digestion at room temperature to limit the likelihood of strong chemical reactions. The final two weeks of sample digestion was aided by a hot water bath set to 50°C; each sample was stirred daily throughout the digestion process, with care taken to ensure that there was no cross contamination between samples. After the H_2O_2 contained in the sample tubes appeared clear in color (indicating most organic matter was dissolved), deionized water (DI) was added to the 50 mL level to begin the rinsing process. The samples were centrifuged at 3500 RPM for 4 min, after which the supernatant liquid was decanted; this process was repeated three times, with new DI water added after each centrifuge cycle to ensure thorough rinsing.

An aliquot of suspended sediment for each 1 cm sample was analyzed using a high-resolution Malvern Mastersizer 3000 laser-particle size analyzer. We use the Wentworth Phi grain size scale to characterize each sample and the statistical software package GRADISTAT to calculate grain size attributes such as the mean grain size, D90 (grain diameter where 90% of the samples grain volume is smaller) and D10 (grain diameter where 10% of the samples grain volume is smaller), and degree of sorting, skewness, and kurtosis to differentiate lithologic units (Blott and Pye, 2001).

3.3 Diatom Analysis

Diatoms found in low-energy intertidal environments are sensitive to changes in salinity and substrate and can therefore be used as proxies for identifying changes in land and/or sea level and

tsunami inundation (Hemphill-Haley, 1996; Shennan et al., 1999; Horton & Sawai, 2010; Dura & Hemphill-Haley, 2020). Diatoms have an important benefit over foraminifera in that diatoms are found throughout the intertidal zone including areas of woody upland, high marsh, low marsh, tidal flat, and subtidal habitats. The presence of a species of diatom is controlled by environmental factors such as temperature, pH, vegetation, salinity, and substrate (Horton et al., 2013; Dura, Hemphill-Haley, et al., 2016).

Because diatoms respond quickly to changes in salinity and substrate, they can record environmental changes caused by coseismic coastal deformation and tsunami inundation in coastal sedimentary sequences (Horton et al., 2017). An increase in marine and/or brackish species in sediments above an inferred tsunami deposit may be interpreted as a positive increase in marine water inundation related to coseismic subsidence. In contrast, a decrease in marine and/or brackish species in sediments above an inferred tsunami deposit may represent coseismic uplift (Hamilton & Shennan, 2005b; Horton et al., 2013). Within a tsunami deposit, the diatom assemblage is often chaotic, containing a mixture of species washed in from a variety of freshwater, brackish, and marine environments as a tsunami inundates the coast.

Following the sample preparation guidelines described by Dura and Hemphill-Haley (2020) and Hemphill-Haley and Lewis (2003), ~1.0 g (~1 cm^3) samples were taken from core W14 close to lithologic contacts at 1 cm intervals and at 15 cm intervals within homogenous layers. Samples were digested with 30% H_2O_2 to remove organic matter, rinsed with deionized water, and centrifuged. A mechanical pipette was used to transfer a specified volume of digested sample (25uL), onto prepared glass cover slips. After drying, the prepared cover slips were mounted sediment-side-down onto labeled glass microscope slides using the mounting material Naphrax

with toluene. A total of 44 microscope slides for core W14 were prepared for diatom microfossil analysis.

Using a Leica light microscope, diatom analysis began with a preliminary scan at 400x to discern diatom concentration and degree of valve fragmentation. Following criteria detailed by (Witter et al., 2009), valves were categorized based on morphology and size classes. To guarantee a representative analysis, a minimum of one completed transect and 300 diatom valves were counted per slide. For each sample, the degree of valve fragmentation was quantified by measuring the ratio of broken to intact valves. A qualitative analysis of diatom valve concentration was measured for each sample.

Species level identification and counting was completed using oil immersion at 1000x magnification. To guarantee a representative assemblage, a minimum of 300 diatoms were identified per sample and represented as a percentage of abundance per sample. For samples containing very high valve concentrations, the first 300 valves were identified at high magnification (1000x) with additional traverses at low (400x) magnification to verify the presence of very large (>100 um) or allochthonous taxa. Fragmented valves were only counted if more than half of the valve was present and identifiable. Core W14 represents a diverse tidal habitat, containing a total of 220 identifiable diatom species. To guarantee ecological provenance is correctly reflected by the diatom assemblages, only species that exceeded 1.5% of total valves counted were used for earthquake and tsunami interpretations. Diatom assemblages were categorized by species salinity preference and preferred tidal habitat, as well as species life-form (planktonic; benthic) based on species ecological preferences outlined in past Alaskan and global studies (Shennan et al., 2009; Shennan, et al., 2014b; Dura, Hemphill-Haley, et al., 2016).

We classify diatom species using the halobian classification scheme of Vos' & de Wolf (1993) which groups diatom species with respect to salinity preferences and the corresponding tidal zone in which they thrive. The polyhalobous assemblage includes marine and marine-brackish diatoms that thrive within the subtidal and tidal zones whose waters commonly exceeds 30 practical salinity units (psu). The mesohalobous assemblage (e.g., brackish-marine, brackish) tolerates a broad spectrum of tidal influence, between 0.2 and 30 psu. The oligohalobous assemblage contains freshwater species that are either tolerant (oligohalobous-indifferent) or stimulated (oligohalobous-halophile) by temporary periods of low salinity (0-0.2 psu). The halophobous assemblage includes freshwater species which thrive in inland waters containing <0.2 psu (Vos' & de Wolf, 1993; Dura, Hemphill-Haley, et al., 2016; Dura & Hemphill-Haley, 2020). The life form of diatom species can benefit depositional environment interpretations and are classified as benthic (attached-living) or planktonic (free-floating). Within the benthic life-forms, there are epiphytic diatom taxa that live attached to coastal plants; taxa that live attached to wet sediments such as sand grains are classified as epipelic; while life-forms that live attached to wet sediment but tolerate briefly dry habitats are aerophilic. Species that live primarily within the benthos but can also be found living in the water column are tychoplanktonic, while planktonic diatoms can be found living freely within the water column (Vos' & de Wolf, 1993).

3.4 Dating Methods

Where possible, plant macrofossils were collected from organic sediment for radiocarbon dating. Dating constrained either limiting minimum (in growth above contact) or maximum (below contact) ages for each of the three sand beds within core W14 as well as adjacent cores W6 and W10. Using methods detailed by Kemp et al. (2013), samples too delicate to withstand transport and/or in situ growth rhizomes were selected for dating. These sampling methods reduce the

potential of dating older material carried inland during tsunami inundation. Using the constrained radiocarbon ages, we calculated the probable age distributions for the three possible tsunami beds represented in core W14.

4. RESULTS

4.1 General Site Stratigraphy

We observed two main lithologic units (unit 1 and 2) and three distinct sand beds within the lower elevation cores of Ocean Bay marsh (Figure 4). In core W14, which is representative of the stratigraphy of the lower portions of Ocean Bay marsh, a dense grey basal sand that contains little to no organic material underlies the marsh between 0.22 and 0.44 m MTL (unit 1). A dark brown, organic rich silty peat overlies the basal sand between 0.44 and 1.27 m MTL. Three sand beds ranging in thickness from 1 to 12 cm are interbedded within unit 2 and extend up to 200 m inland and at least ~150 m laterally across the lower elevations of Ocean Bay marsh. Labeled from oldest to youngest, sand beds C, B, and A were easily distinguished from surrounding sediments due to their sharp (<1-3 mm) upper and lower contacts, uniform thickness, lateral extent, lack of organic matter, and presence of abundant epipsammic marine microfossils.

4.2 Detailed Analysis of Core OBL.15.W14

4.2.1 Sand bed C and under- and over-lying units

Between 0.52 and 0.605 m MTL, a dark brown, very poorly sorted, organic-rich silty peat (unit 2; mean = 5.4 Φ; D10 = 8.2 Φ) underlies sand bed C (Figure 5). Fresh-brackish benthic diatom species *Pinnularia lagerstedtii (17%)*, *Stauroforma exiguiformis (11%),* and *Cosmioneis pusilla (*7%*)*, and the benthic brackish species *Navicula peregrina (10%)* are most common in the silty peat underlying sand bed C (Figure 6).

At 0.605 m MTL, a sharp contact separates unit 2 from sand bed C, a 1-cm thick, grey, poorly sorted fine quartz sand (mean = 2.8 Φ; D10 = 5.6 Φ). An increase in mean grain size and a decreased fine fraction—shown by a decrease in D10 value—distinguishes sand bed C from the under- and overlying silty peat of unit 2. The diatom assemblage within sand bed C is dominated

by marine (75%) and fresh (22%) species, with a near total absence of brackish diatoms (<1%). Compared to the underlying unit 2, sand bed C contains abundant epipsammic marine-brackish species (e.g., *Opephora sp* (44%) and *Planothidium delicatulum* (10%)). The concentration of diatom valves within sand bed C is significantly lower than both the under- and overlying sediments, with multiple traverses completed to reach the representative 300-valve minimum. The degree of fragmentation of diatom valves is subtly higher within sand bed C than the surrounding sediments (Figure 7). Calibrated radiocarbon dating of a dark rhizome sampled from the sediment underlying sand bed C constrains the age of deposition to 494-329 cal yr B.P. (A.D. 1526-1691).

A sharp upper contact at 0.615 m MTL separates sand bed C from the overlying silty peat of unit 2 (mean = 5.03 Φ; D10 = ~8.1 Φ). The diatom assemblage overlying sand bed C is characterized by a mixed assemblage of fresh-brackish and marine-brackish species. Fresh-brackish species *Pinnularia lagerstedtii* (12%) and *Stauroforma exiguiformis* (12%) dominate, alongside the epipsammic marine diatom *Opephora* sp (6%). Compared to the silty peat underlying sand bed C, there is a 5% decrease in the fresh-brackish diatoms *Pinnularia lagerstedti* and *Cosmioneis pusilla*, as well as a small (<3%) increase in the abundance of marine taxa such as *Thalassionema nitzschioides, Thalassiosira eccentrica,* and *Odontella aurita*..

4.2.2 Sand bed B and under- and over-lying units

Between 0.615 and 0.70 m MTL, unit 2 (mean = 5.03 Φ; D10 = 8.1 Φ) underlies sand bed B (Figure 5). The diatom assemblage underlying sand bed B is dominated by fresh-brackish species (totaling 54%) including *Pinnularia lagerstedtii* (11%), *Cosmioneis pusilla* (7%), and *Stauroforma exiguiformis* (9%). The remaining diatom assemblage within the silty peat below sand bed B includes low abundances of marine-brackish (total 15%) and brackish (total 9%) species.

At 0.70 m MTL, a sharp lithologic contact separates unit 2 from sand bed B. Sand bed B is 12 cm thick and composed of grey, moderately-poorly sorted, fine quartz sand (mean = 2.45 Φ; D10 = 4.36 Φ). An increase in mean grain size and a decreased fine fraction—shown by a decrease in D10 value—distinguishes sand bed B from the under- and overlying silty peat of unit 2. Twelve grain-size samples taken at 1 cm vertical intervals indicate subtle inverse grading throughout sand bed B, illustrated by a decrease in fine-fraction (from 2.73 Φ to 2.28 Φ) with reduced depth. The diatom assemblage within sand bed B is characterized by abundant marine epipelic (*Diploneis interrupta*; 32%), marine epipsammic (*Opephora sp*; 10%), and fresh-brackish species (e.g., *Stauroforma exiguiformis*; 6%) (Figure 6). In comparison with the surrounding silty peat, the concentration of diatom valves within sand bed B is significantly lower, and the degree of valve fragmentation is subtly higher (Figure 7). Calibrated radiocarbon dating of a woody steam entrapped within the sediment directly below sand bed B constrains the age of deposition to 290-0 cal yr B.P. (AD 1730-0).

A sharp upper contact at 0.82 m MTL separates sand bed B from the overlying silty peat of unit 2 (mean = 4.51 Φ; D10 = 7.85 Φ). Within the silty peat overlying sand bed B, there is an increase in brackish (e.g., *Navicula peregrina* up 11%; *Diploneis pseudovalis* up 8%) and marine (e.g., *Diploneis smithii* up 4%; *Opephora sp* up 3%) taxa compared to the fresh-brackish dominated assemblage in sediments underlying sand bed B. The increases in brackish and marine taxa are accompanied by decreases in fresh-brackish species (e.g., *Pinnularia lagerstedtii* down 7%; *Cosmioneis pusilla* down 6%), supporting an increase in marine and brackish influence above sand bed B.

4.2.3 Sand bed A and under- and over-lying units

Between 0.82 and 1.08 m MTL, unit 2 (mean = 2.94 Φ; D10 = 5.48 Φ) underlies sand bed A (Figure 5). The diatom assemblage underlying sand bed A is dominated by fresh-brackish diatom species (totaling 52 %) including *Pinnularia lagerstedtii* (15%), *Stauroforma exiguiformis* (6%), and *Caloneis bacillum* (5%). The remaining assemblage within the silty peat below sand bed A includes similar taxa to those underlying sand bed B (i.e., *P. lagerstedtii* 15%, *S. exiguiformis* 6%) (Figure 6).

At 1.08 m MTL, a sharp lithologic contact separates unit 2 from sand bed A. Sand bed A is 6.5 cm thick and composed of grey, poorly sorted, fine quartz sand (mean = 2.94 Φ; D10 = 5.48 Φ). An increase in mean grain size and a decreased fine fraction—shown by a decrease in D10 value—distinguishes the grain size of sand bed A from the under- and overlying silty peat of unit 2. Six grain-size samples taken at 1 cm intervals display an increased fine fraction toward the top of the bed, indicating upward fining. The diatom assemblage within sand bed A is characterized by a mixed assemblage of marine epipsammic (e.g., *Opephora sp*; 9%), brackish epipelic (e.g., *Navicula peregrina*; 11%) and epiphytic (e.g., *Ctenophora pulchella*; 10%), and fresh-brackish (e.g., *Mastogloia elliptica*; 7%) species. Similar to sand beds C and B, sand bed A displays a subtle increase in diatom valve fragmentation, but contains a significantly higher concentration of valves than sands C and B. Based on widespread historical observations of tsunami inundation of Kodiak Island following the 1964 earthquake, we infer sand bed A was deposited by that event.

A sharp upper contact at 1.145 m MTL separates sand bed A from the overlying silty peat of unit 2 (mean = 4.33 Φ; D10 = 7.39 Φ). Within the silty peat overlying sand bed A, there is an increase in marine (e.g., *Surirella brebissonii* and *O. marina* up 4%) and brackish (*Navicula peregrina* up 8%; *Pinnunavis elegans* up 6%) taxa compared to the fresh-brackish dominated

assemblage in sediments underlying sand bed A. Additionally, there are subtle (<3%) increases in marine planktonic (e.g., *Actinoptychus senarius*; *Thalassiosira pacifica)* and tychoplanktonic (e.g., *Cyclotella meneghiniana*) taxa above sand bed A. The increases in marine and brackish taxa are accompanied by decreases in fresh-brackish (down 25%) diatoms (Figure 8), supporting an increase in marine and brackish influence above sand bed A.

5. DISSCUSSION

Based on stratigraphy, lithology, diatom, and radiocarbon analyses, we reconstruct the environmental changes preserved in the lower elevation cores of Ocean Bay marsh over the last ~400 years. Diatom assemblages in core W14 indicate that over the last ~400 years, the environmental conditions at Ocean Bay marsh were similar to those of today. However, within this overall pattern of stability, diatoms fluctuate between freshwater and/or fresh-brackish dominated assemblages and marine and/or brackish dominated assemblages punctuated by widespread, anomalous sand beds. Below, we interpret the sand beds to have been deposited by tsunamis and infer that the sudden and lasting environmental changes associated with two of the sand beds signal sudden RSL rise during times of decimeter-scale coseismic subsidence.

5.1 Evidence for tsunami deposition

We infer a tsunami origin for sand beds C, B, and A preserved within the lower elevation stratigraphy of Ocean Bay marsh. Our interpretations are based on shared characteristics within all three sand beds, including widespread lateral extent, sharp upper and lower contacts, anomalously coarse grain size, and mixed diatom assemblages that include abundant marine epipsammic species. Similar characteristics have been documented in modern tsunami deposits worldwide, including in Chile (e.g., Cisternas et al., 2017; Dura et al., 2017), Japan (e.g., Sawai et al., 2012), Thailand (e.g., Jankaew et al., 2008), and Cascadia (e.g., Witter et al., 2003; Nelson et al., 2020).

Sand beds C, B, and A can be correlated over distances of ~20-200 m within Ocean Bay marsh and drape over the existing paleo-topography. Sand bed A displays upward fining and an increased fine fraction near the top of the bed, a feature indicating sediment settling out of suspension after tsunami flow deceleration (Dawson & Shi, 2000; Morton et al., 2007). In sand bed B, subtle inverse grading, represented by a decreased fine fraction near the top of the bed, may be explained through

variation in tsunami wave velocity and/or topography during deposition (Dawson & Stewart, 2007; Shanmugam, 2012; Garrett et al., 2015). The lateral continuity and lithologic characteristics of the sand beds helps rule out localized processes like tidal channel migration or liquefaction during earthquakes as the responsible mechanism for sand bed deposition (Atwater, 1987; Morton et al., 2007).

We interpret the mixed diatom assemblages within sand beds C, B, and A to be indicative of tsunami inundation across the subtidal, intertidal, and supratidal environments of Ocean Bay marsh (Hemphill-Haley, 1996; Horton et al., 2013; Dura & Hemphill-Haley, 2020). The presence of abundant epipsammic marine diatoms (i.e., *P. delicatulum, O. marina*) within the sand beds suggests that the tidal flats and/or subtidal channels bordering the marsh were the primary sources of coarse sediment (Hemphill-Haley, 1996). Higher rates of diatom valve fragmentation in all three sand beds, and low valve concentration in two of the beds (bed A excluded), corroborate high-energy deposition (Witter et al., 2009; Dura & Hemphill-Haley, 2020).

5.2 Evidence for abrupt, regional, and persistent subsidence

The diatom analysis for core W14 indicates abrupt, lasting RSL rise associated with deposition of sand beds B and A, which we infer was caused by coseismic subsidence. Our interpretations are consistent with similar coastal geologic studies that also used diatoms as a proxy to infer coseismic subsidence (Hemphill-Haley, 1996; Zong et al., 2003; Witter et al., 2009; Dura et al., 2017). However, in contrast to many previous studies, the Ocean Bay marsh stratigraphy does not display significant lithologic changes coincident with diatom evidence of subsidence. The silty peat under- and overlying sand beds B and A is mostly homogenous, with minimal variation in grain size and organic content below and above the sand beds. This observation is consistent with modern research of clastic-dominated marshes that show little change in lithology between

high and low marsh settings and suggests that although coseismic subsidence within a high to low intertidal marsh environment may not be lithologically apparent, diatoms can still display a response to increased tidal inundation (Horton et al., 1999; Hawkes et al., 2010; Dura et al., 2015).

We observed increases in marine and/or brackish diatoms within the silty peat units overlying two of the three sand beds (B and A) consistent with coseismic subsidence (Figure 8). The subtle increases in marine diatoms observed above sand bed C are not significant enough to infer coseismic subsidence coincident with sand bed deposition. The silty peat underlying sand beds B and A is generally dominated by a diverse assemblage of high-marsh fresh-brackish epipelic diatoms (i.e., *P. lagerstedtii*, *S. exiguiformis, C. pusilla*). Within the silty peat overlying sand beds B and A, there is an increase in epipsammic marine species (i.e., *O. marina*) and brackish epipelic species (i.e., *N. peregrina*) paired with decreases in fresh-brackish species (i.e., *C. pusilla, P. lagerstedtii*), suggesting increased tidal inundation of the marsh resulting from coseismic subsidence (Hemphill-Haley, 1996; Dura, Hemphill-Haley, et al., 2016).

The diatom assemblages within the silty peat units overlying sand beds B and A display a lasting shift in ecology that persists for several centimeters, ruling out temporary sea-level fluctuations (Horton & Sawai, 2010; Horton et al., 2017). The increased abundance of marine and/or brackish species overlying the sand beds is then followed by the slow return of fresh-brackish species and a decrease in marine species that suggests RSL fall, consistent with gradual interseismic uplift.

The evidence for coseismic subsidence coincident with sand beds B and A strengthens our interpretation of sand bed deposition by tsunamis produced by large, regional subduction zone earthquakes rather than storms. Although we acknowledge that storm overwash events can deposit widespread sand beds (e.g., Soria et al., 2017), evidence for coseismic subsidence and the

correlation of tsunami and land-level change evidence over hundreds of kilometers (outlined in more detail below) helps rule out more localized storm overwash processes (Nelson et al., 1996; Dawson & Stewart, 2007).

5.3 Regional correlation of Ocean Bay marsh seismic events and implications for trench-parallel and trench-perpendicular slip distributions

The vertical deformation experienced on coastlines during the coseismic period is controlled by the geometry, amount, and spatial distribution of slip along the megathrust fault plane. The distribution of coseismic slip often varies in each earthquake, allowing the pattern and amount of deformation to vary at one coastal location (Plafker, 1965; Wang et al., 2013; Briggs et al., 2014). A coast-perpendicular coseismic slip model for the Kodiak region indicates that shallower (0-20 km), seaward, slip will result in coseismic subsidence at Ocean Bay marsh, while deeper (20-40 km), more landward slip will result in uplift (Suleimani et al., 2017; Shennan et al., 2018). Slip occurring at an intermediate depth (10-30 km) will result in a hinge line for uplift and subsidence (zero-contour) falling just seaward of Ocean Bay marsh (Suleimani et al., 2017). In the sections below, we use this general slip model and our radiocarbon analyses to put the timing of tsunami deposition and coseismic subsidence into a chronological and regional tectonic framework.

5.3.1 Prehistoric earthquake and tsunami: 400 cal yr B.P. (sand bed C)

Maximum ages from below sand bed C in core W14 (494-329 cal yr B.P), W10 (308-0 cal yr B.P.), and W6 (456-311 cal yr B.P.) overlap with the regional ~400 cal yr B.P. earthquake, thus we attribute sand bed C to that event. Stratigraphic and diatom evidence support tsunami inundation of Ocean Bay marsh associated with the ~400 cal yr B.P. earthquake. We found little to no evidence for coseismic subsidence coincident with sand bed deposition; the diatom

assemblage above sand bed C does not significantly differ from the underlying silty peat, nor is there an apparent change in lithology.

The lack of evidence for coseismic deformation at Ocean Bay marsh correlates with observations at other along-strike sites in eastern Kodiak Island that do not record deformation (e.g., Middle Bay, Anton Larson Bay, and Kalsin Bay) associated with the ~400 cal yr B.P. earthquake (Shennan et al., 2014a). Evidence of coseismic subsidence further eastward and landward at Shuyak (Shennan et al., 2014a; Shennan et al., 2018), and evidence of coseismic uplift and tsunami inundation westward and trenchward of Sitkalidak at Sitkinak Island (Briggs et al., 2014) suggests our study area at Ocean Bay marsh lies at or near the zero-contour (i.e., hingeline) of coseismic deformation (Figure 3), and that the event produced intermediate depth slip at Sitkalidak Island (Figure 3d).

Based on our results and regional geologic evidence, the 400 cal yr B.P. earthquake encompassed at least the Kodiak segment of the subduction zone. However, constraining the rupture to only the Kodiak segment is complicated by the potential overlap of similarly dated events recorded further eastward on the Kenai segment (422-0 cal yr B.P.; Kelsey et al., 2015), in northwestern Kodiak (500-300 cal yr B.P.; Gilpin, 1995), and westward on the Semidi segment (510-317 cal yr B.P.; Nelson et al., 2015). Geologic evidence for the 400 cal yr B.P. event in the Kodiak segment is not suggestive of a large, multi-segment rupture (i.e., 1964 Mw 9.2) that would account for evidence in all three segments; evidence for coseismic subsidence and tsunami inundation is scarce, subtle, and not well constrained. It is likely that multiple earthquakes occurred in the 500-400 cal yr B.P. timeframe, underscoring the need for more geologic investigations and better age control on earthquake and tsunami events documented in the western Kodiak and Semidi segments (Gilpin, 1995; Carver & Plafker, 2008; Shennan et al., 2018).

5.3.2 Historic earthquake and tsunami: AD 1788 (sand bed B)

Maximum ages from below sand bed B in core W14 (290-0 cal yr B.P.) and W10 (308-0 cal yr B.P.) overlap with the regional AD 1788 earthquake and tsunami, thus we attribute sand bed B to that event. Our stratigraphic and diatom evidence supports tsunami inundation of Ocean Bay marsh associated with the 1788 earthquake. Although there is no change in lithology above sand bed B, an increase in brackish diatom species and simultaneous decreases in freshwater species above the sand bed indicate coseismic subsidence occurred coincident with sand bed deposition.

Our evidence for tsunami inundation and coseismic subsidence at Ocean Bay marsh correlates with observations at other along-strike sites in the eastern Kodiak region that record subsidence with or without tsunami inundation (e.g., Shuyak, Middle Bay, Kalsin Bay, Settlement Point) associated with the 1788 earthquake (Shennan et al., 2014a; Shennan et al., 2018). This correlative evidence paired with Briggs et al. (2014) observations of coseismic uplift further trenchward at Sitkinak suggests the hingeline for the 1788 earthquake was located offshore of Sitkalidak Island, and that the event produced intermediate to shallow slip at Sitkalidak (Figure 3c).

The presence of tsunami and earthquake evidence at Ocean Bay marsh, Sitkinak Island, and Chirikof Island supports the Briggs et al., (2014) conclusion that the 1788 rupture propagated through the proposed rupture boundary between the 1938 and 1964 ruptures (Wesson et al., 2007). Based on our results and regional geologic evidence, the 1788 earthquake encompassed the Kodiak and at least the eastern end of the Semidi segment (Briggs et al., 2014; Shennan et al., 2014a). However, constraining the far western extent of the 1788 rupture is complicated by incomplete and potentially false historical records (Engelhart et al., 2018) and difficulty dating the event due to the radiocarbon age plateau (Garrett et al., 2015). Historical accounts of the 1788 earthquake

and tsunami suggest the most severe inundation occurred much further (>400 km) westward in the Shumagin and Sanak islands, yet no evidence of tsunami inundation nor coseismic deformation has been found there for this event (Witter et al., 2014), underscoring the necessity for more investigation of the western megathrust segments.

5.3.3 Historic earthquake and tsunami: AD 1964 (sand bed A)

Ample evidence exists for widespread tsunami inundation coincident with coseismic subsidence of northern Sitkalidak and uplift of the extreme southeast and southwest coasts during the 1964 earthquake (Carver et al., 1992; Plafker, 1965; Kachadoorian & Plafker, 1967). Based on regional correlations and dating of the lower two sand beds, we infer sand bed A to be associated with the 1964 earthquake. Although lacking any apparent change in lithology, an abrupt increase in marine and brackish diatoms and simultaneous decrease in freshwater species above sand bed A indicates coseismic subsidence coincident with sand bed deposition.

Our evidence for tsunami inundation and coseismic subsidence at Ocean Bay marsh is consistent with observations at other along-strike sites in the eastern (e.g., Shuyak, Middle Bay, Kalsin Bay, Settlement Point) Kodiak region that record subsidence and tsunami inundation (Shennan et al., 2014a; Shennan et al., 2018). This correlative evidence suggests that the hingeline for the 1964 earthquake was offshore of Sitkalidak, like the 1788 event, and that the event produced intermediate to shallow slip at Sitkalidak. However, subsidence observed at Sitkinak associated with the 1964 earthquake, where we would expect uplift, suggests more complex rupture processes at play. Briggs et al. (2014) interpretated the subsidence observed on the south side of Sitkinak as the result of a subsidence trough wrapping around the primary zones of uplift. This observation places Sitkinak at the western termination of the 1964 rupture.

Our evidence of coseismic subsidence and tsunami inundation contrasts with previous observations that place Ocean Bay marsh along the axis of zero deformation for the 1964 earthquake (Plafker, 1969). Inconsistencies in quality and scale of graphic representations of the zones of uplift and subsidence for the 1964 earthquake complicate our interpretations for the location of the axis of deformation (Plafker, 1965, 1969; Eckel, 1970). Based on stratigraphic and microfossil results from Ocean Bay marsh, we propose that the axis of deformation (e.g.hingline) for the AD 1964 earthquake lies offshore (3-4 km) from Ocean Bay marsh and may pass through the very southeastern and western tips of Sitkalidak Island (Figure 3b). The relatively small distance (10-20 km) between subsidence at Ocean Bay marsh (this paper) and uplift of the far southeastern and southwestern coasts of Sitkalidak (Plafker, 1965), helps verify the placement of trench-perpendicular deformation zones for the 1964 earthquake.

6. CONCLUSION

Using lithology, stratigraphy, radiocarbon dating, and diatom micropaleontology, we identified three instances of tsunami inundation over the last ~400 years, two of which were coincident with coseismic subsidence. Three widespread anomalously coarse-grained sand beds display both lithologic and diatom characteristics indicative of high-energy, marine-sourced tsunami deposition dated to ~400 cal yr B.P., AD 1788, and AD 1964. Diatom analysis suggests coseismic subsidence coincident with tsunami inundation for the 1964 and 1788 earthquakes, consistent with detailed historic observations and previous coastal studies.

Our investigation at Ocean Bay marsh helps better define the trench-parallel rupture extent and trench-perpendicular zone of deformation for three earthquakes and tsunamis occurring in ~400 cal yr B.P., 1788, and 1964. The close spacing of these three events helps define the spatial distribution and depth of slip on the Kodiak and Semidi segments of the Alaska-Aleutian subduction zone, as well as providing better constraints for rupture and tsunami modeling important to natural hazard analysis. Understanding the mechanisms driving these events have important implications for assessing earthquake hazards associated with the Alaska-Aleutian subduction zone throughout prehistoric time-scales.

APPENDIX A

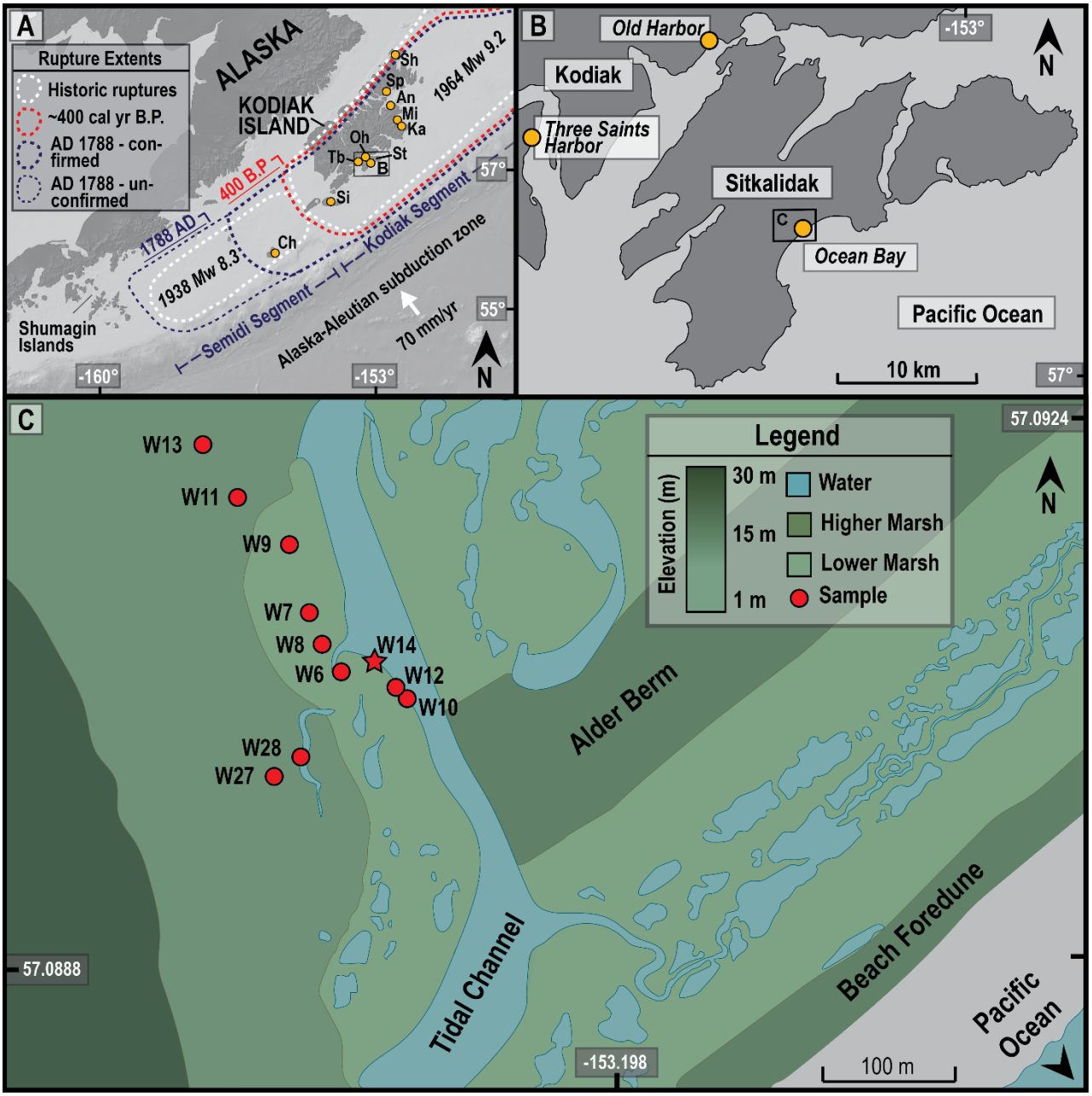

Figure 1. (a) regional map of Alaska and the Kodiak Island region showing locations of correlated sites and proposed rupture extents for historic and prehistoric earthquakes. Focus box **B** marks Sitkalidak Island (b) Sitkalidak Island and southwestern Kodiak Island. Focus box **C** marks Ocean Bay marsh. (c) Ocean Bay marsh site map showing sediment core locations. Core W14 chosen for detailed analysis. (Sh=Shuyak Island; Sp=Settlement Point; An=Anton Larson Bay; Mi=Middle Bay; Ka=Kalsin Bay; St=Sitkalidak Island; Oh=Old Harbor; Tb=Three Saints Bay; Si=Sitkinak Island; Ch=Chirikof Island)

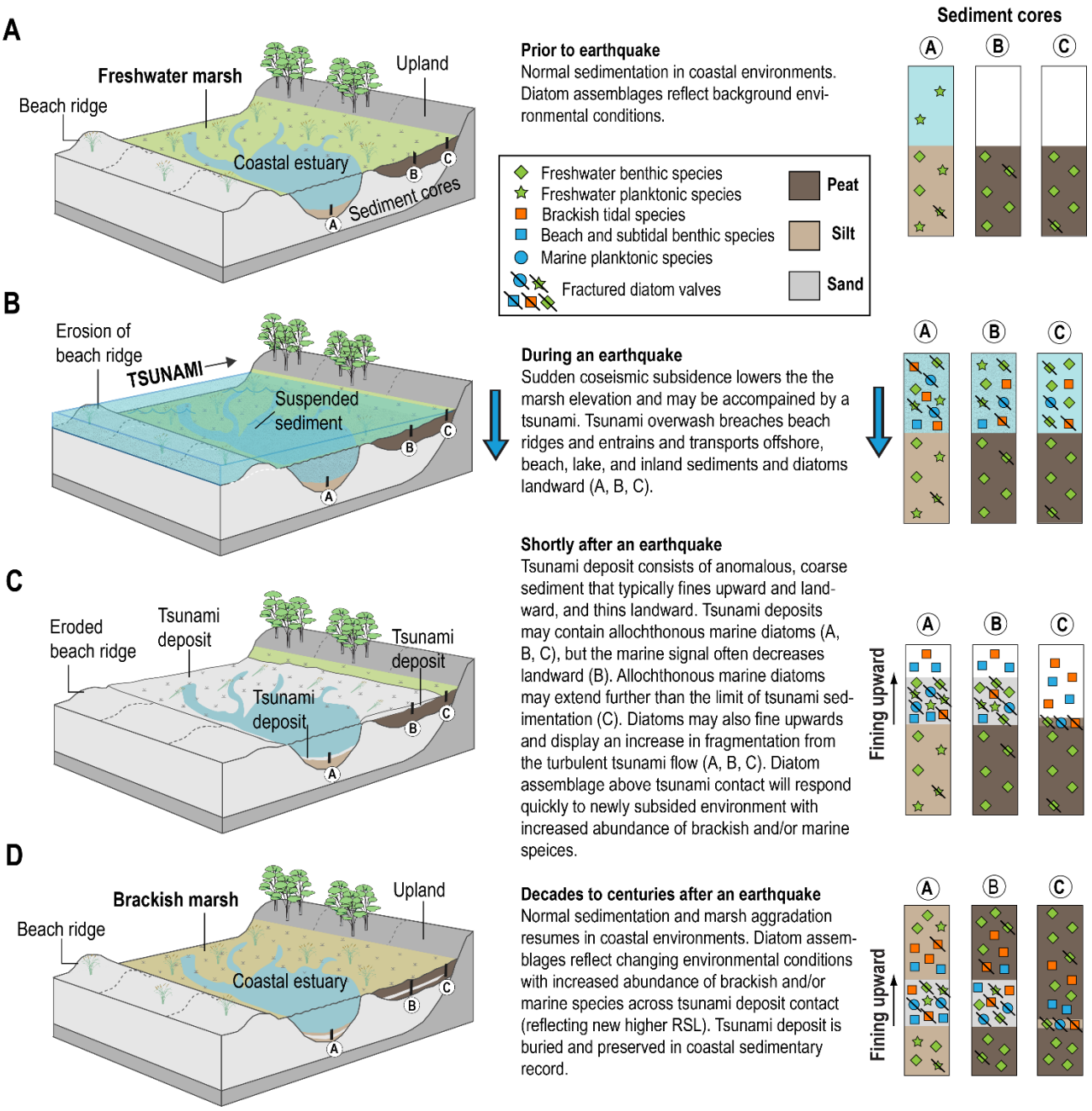

Figure 2. Simplified depiction of stratigraphic and diatom signals for an earthquake which produced coseismic subsidence and tsunami inundation at a coastal freshwater marsh. (a) a coastal freshwater marsh experiencing normal sedimentation; diatoms reflect environmental conditions. (b) coseismic subsidence during the earthquake lowers the land-level and tsunami overwash entrains and deposits sediment and diatoms. (c) tsunami deposits anomalously coarse sediment and allochthonous marine diatoms; diatoms respond quickly to newly subsided environment. (d) sedimentation continues, burying the tsunami deposit; increased marine/brackish diatoms above tsunami deposit reflect changing environment. Modified from Dura et al. (2020).

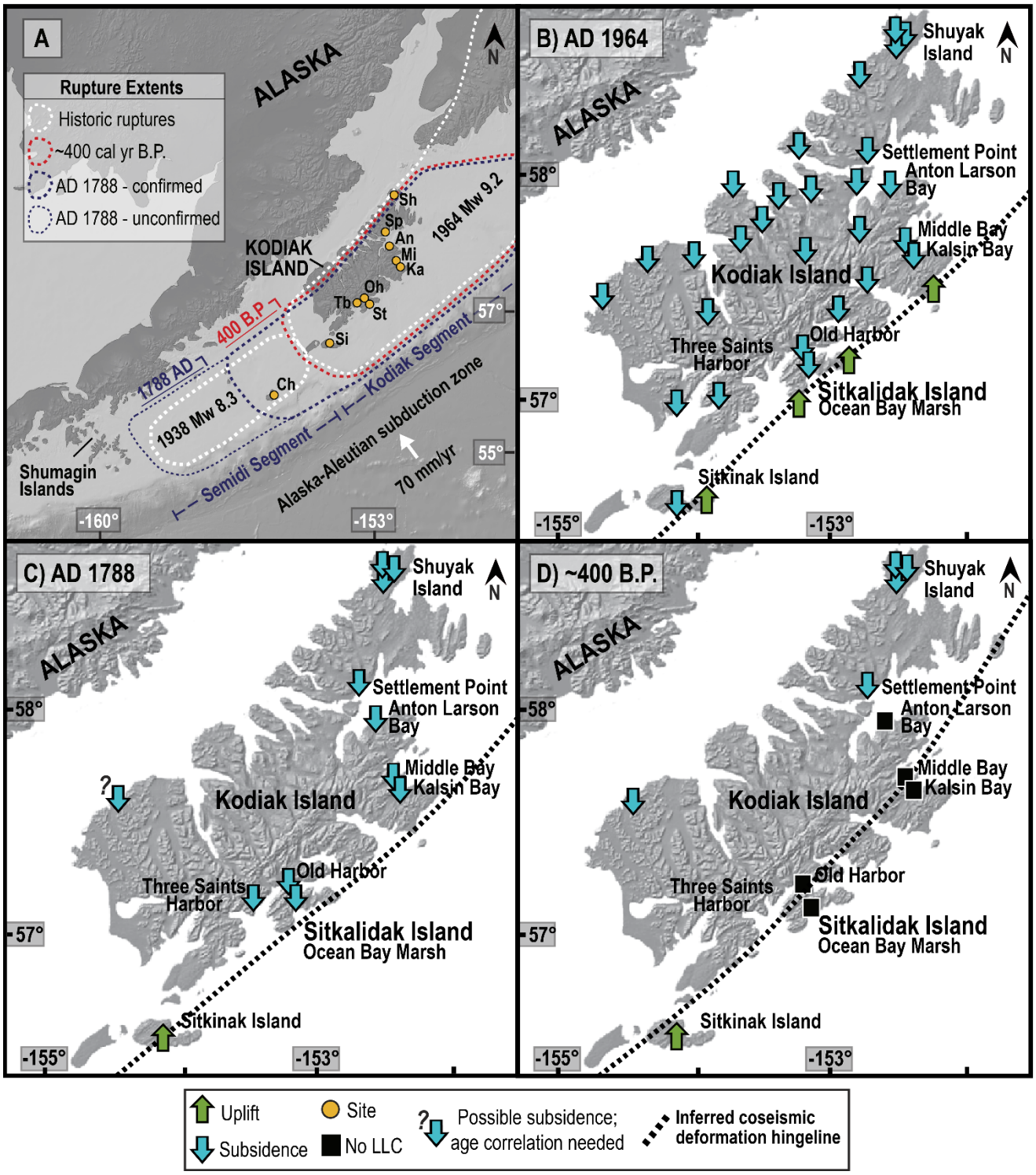

Figure 3. Summary of regional coseismic deformation inferred from stratigraphy and microfossil studies and proposed axis of deformation (e.g., hingeline) for the AD 1964, AD 1788, and 400 cal yr B.P. earthquakes. Modified from Shennan et al. (2014, 2018).

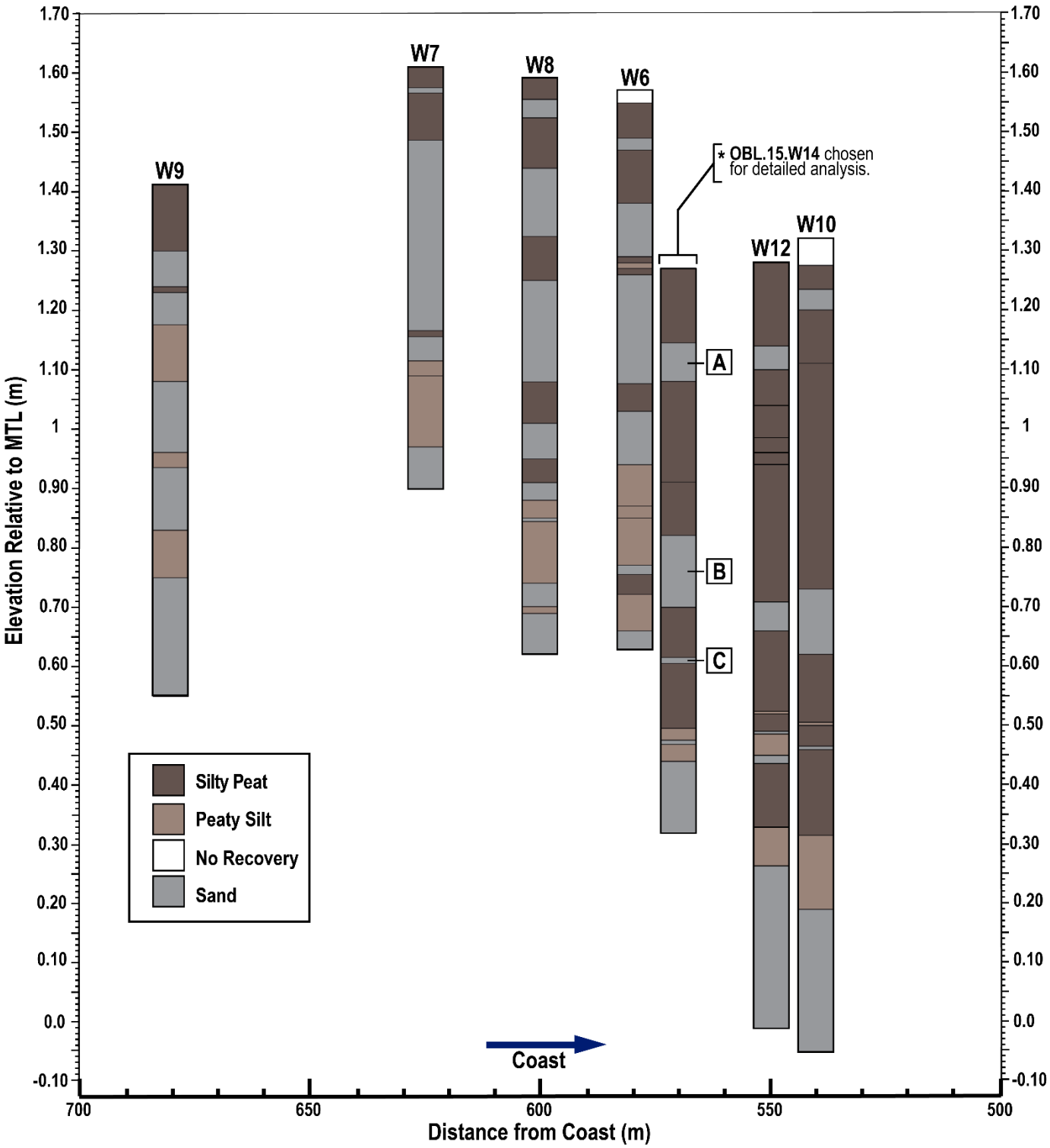

Figure 4. Simplified stratigraphic cross section showing sediment cores from the lower elevation surface of Ocean Bay marsh. Elevation adjusted to mean tide level (MTL). Core OBL.15.W14 selected for detailed analysis. From 1.27 – 0.52 MTL, core W14 records tsunami sands associated with the AD 1964, AD 1788, and ~400 cal yr B.P. earthquakes, labeled A, B, and C, respectively.

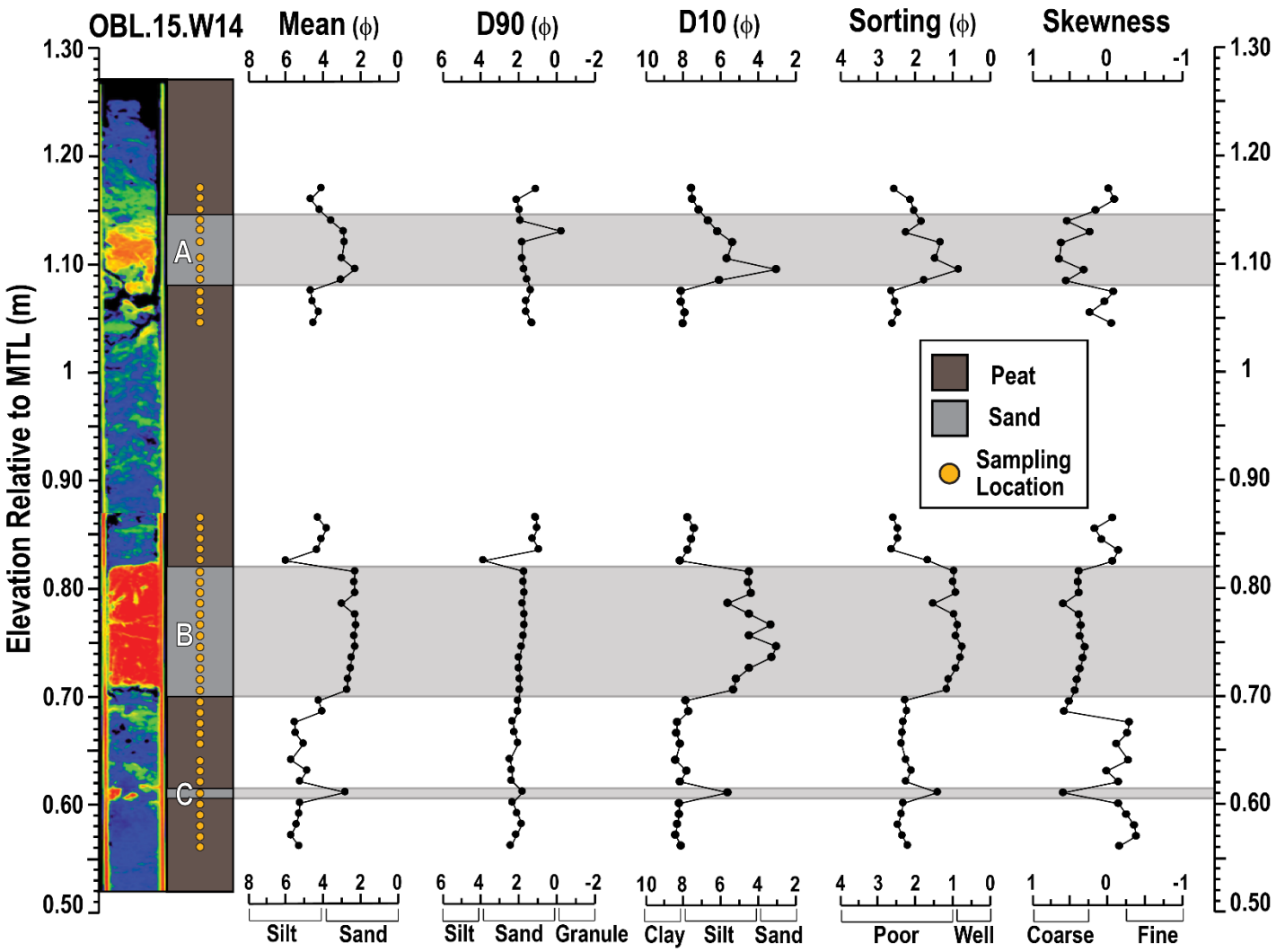

Figure 5. Grain-size summary for core OBL.15.W14. From left to right: CT scan of W14 showing anomalously coarse sediment in reds and oranges and finer grained silt and clay grains in blues and purples; simple stratigraphic column showing lithology and sampling locations; grain-size plots.

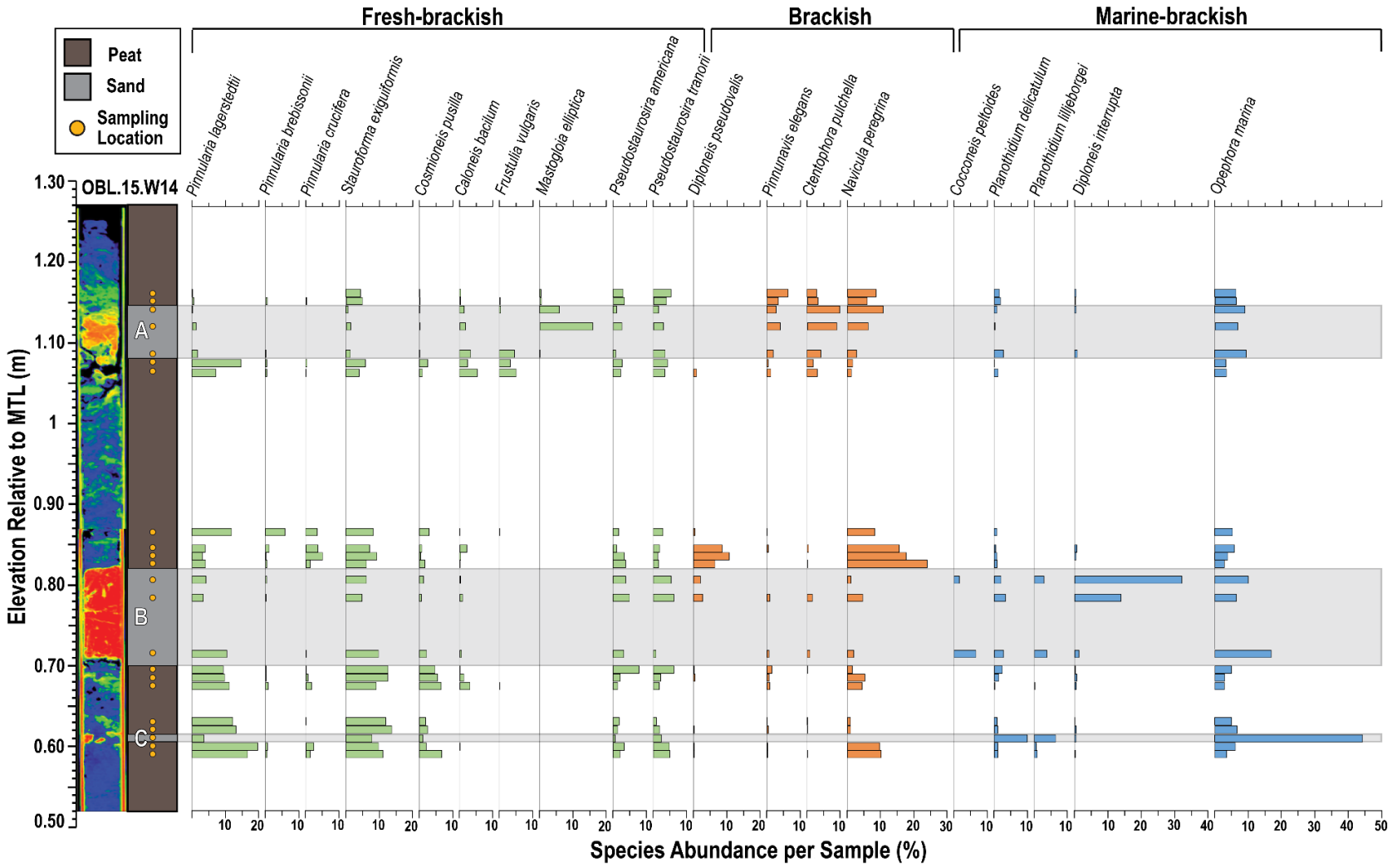

Figure 6. Diatom summary for Ocean Bay marsh (core W14) showing species over 5% abundance for at least on sample. Diatom assemblages grouped by salinity tolerance.

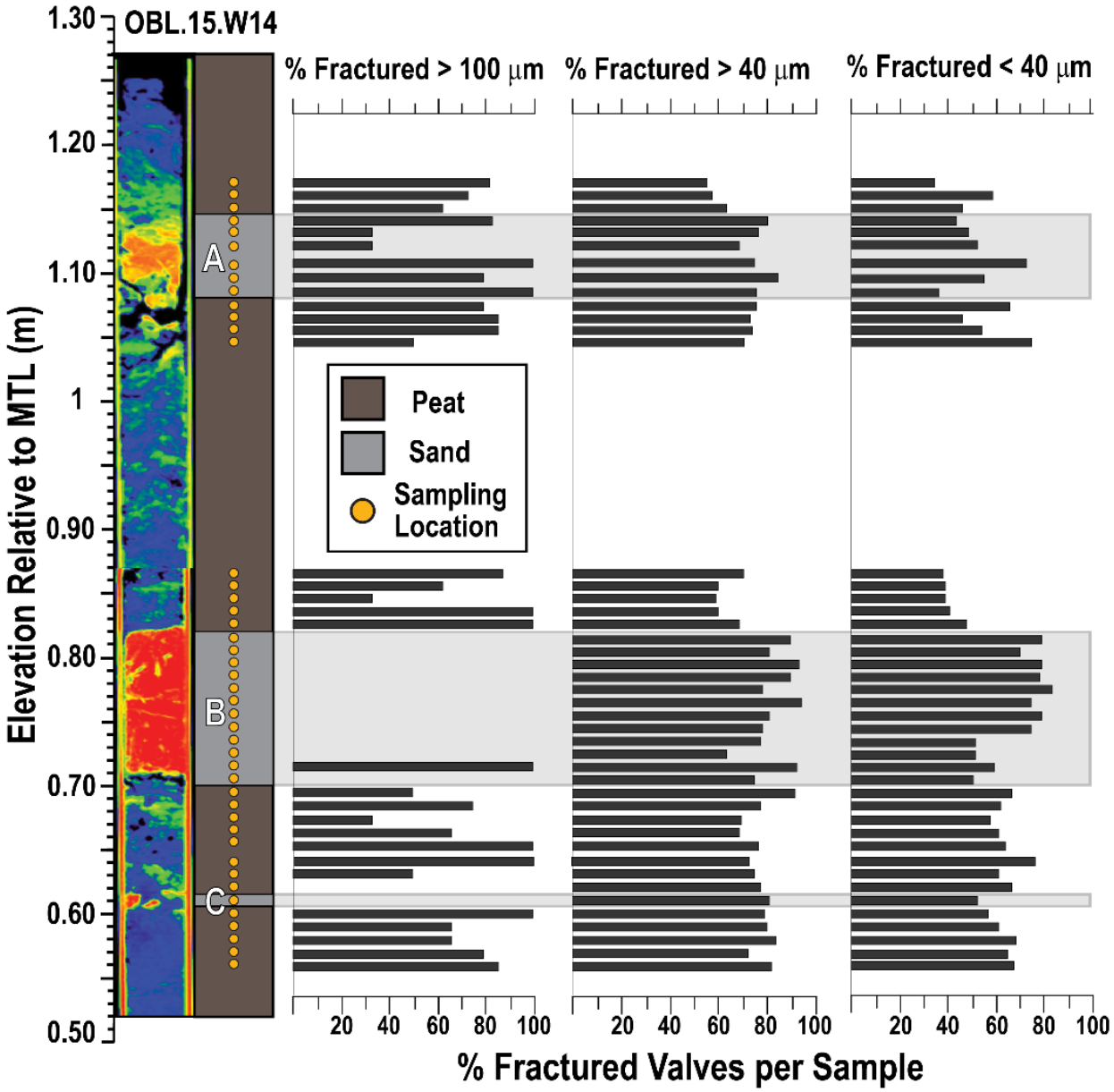

Figure 7. Percent of fractured diatom valves per sample and categorized into size classes. Increased valve fragmentation rate within sand beds best seen within sand bed B. Absence of data in the >100 um column is caused by a total lack of diatoms of that size class seen in some samples.

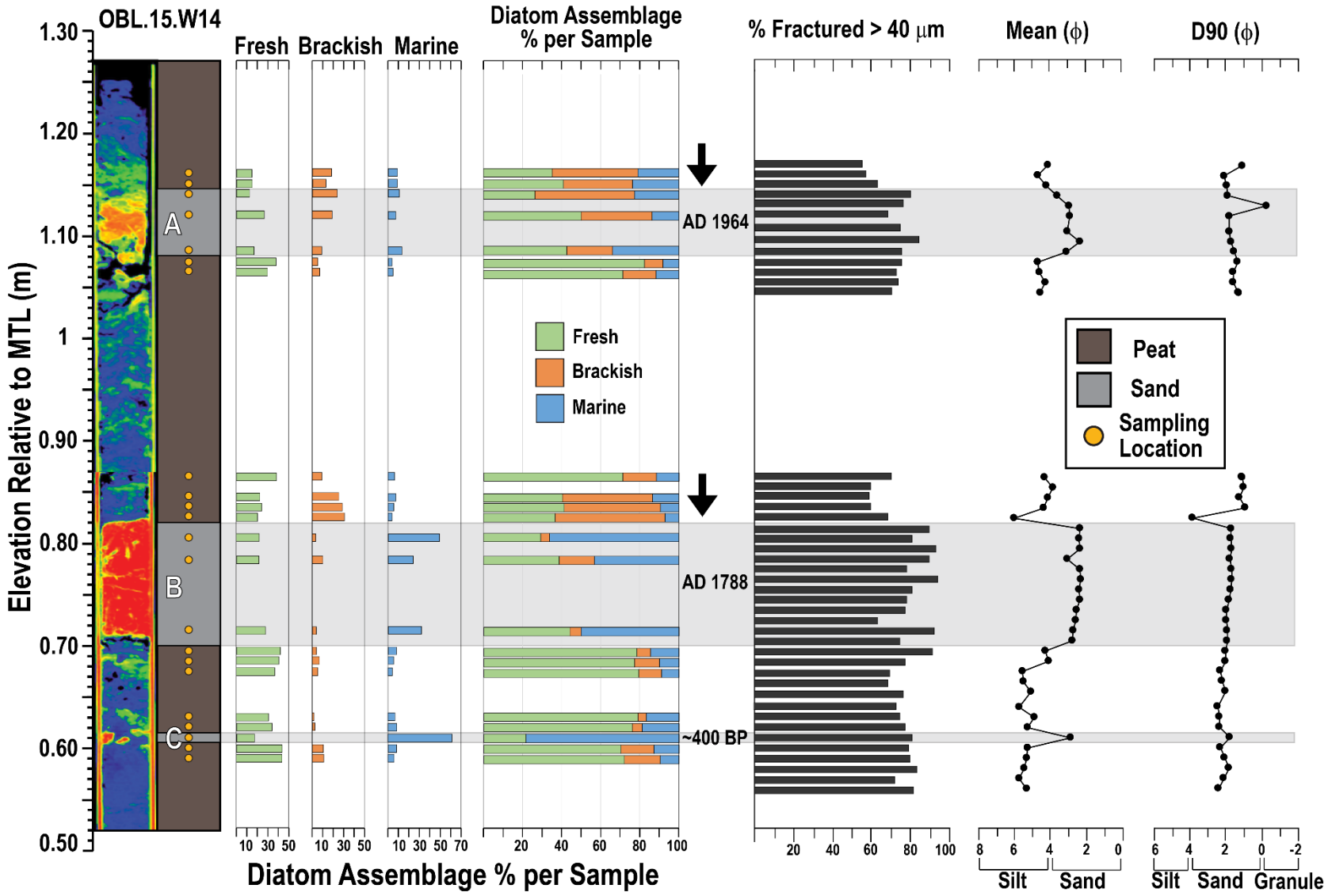

Figure 8. Diatom and grain-size summery. Diatom data presented as percent abundance per sample for fresh, brackish, and marine assemblages categorized by individual species environmental preferences. Diatom statistics reflect species constituting 5% or more of a at least one sample.

Table 1. Summary of AD 1964, AD 1788, and c.400 BP earthquake and tsunami evidence. 1- Prater et al (2021); 2- Shennan et al (2014); 3- Shennan et al (2018); 4- Plafker (1965), Janigan et al (2018); 5- Briggs et al (2014); 6- Soloviev (1990); 7- Nelson et al (2015)

	Eastern Kodiak Region					Western Kodiak Region				
Calibrated age	Shuyak[3] Island	Settlement Point[2]	Anton Larson Bay[2]	Middle Bay[2]	Kalsin Bay[2]	Sitkalidak - Ocean Bay[1]	Old Harbor[4]	Sitkinak[5]	Three Saints Harbor[6]	Chirikof Island[7]
AD 1964	T & S	T & S	T & S	T & S	T & S	T & S	T & S	T & S	T & S	no evidence
AD 1788	S	T & S	S	S	T & S	T & S	T	T & U	T & S	T
c.400 BP	*T & S	S	no evidence	no evidence	no evidence	T	no evidence	T & U	N/A	*T

T - tsunami	*T - possible tsunami
S - subsidence	*S - possible subsidence
U - uplift	N/A - not investigated

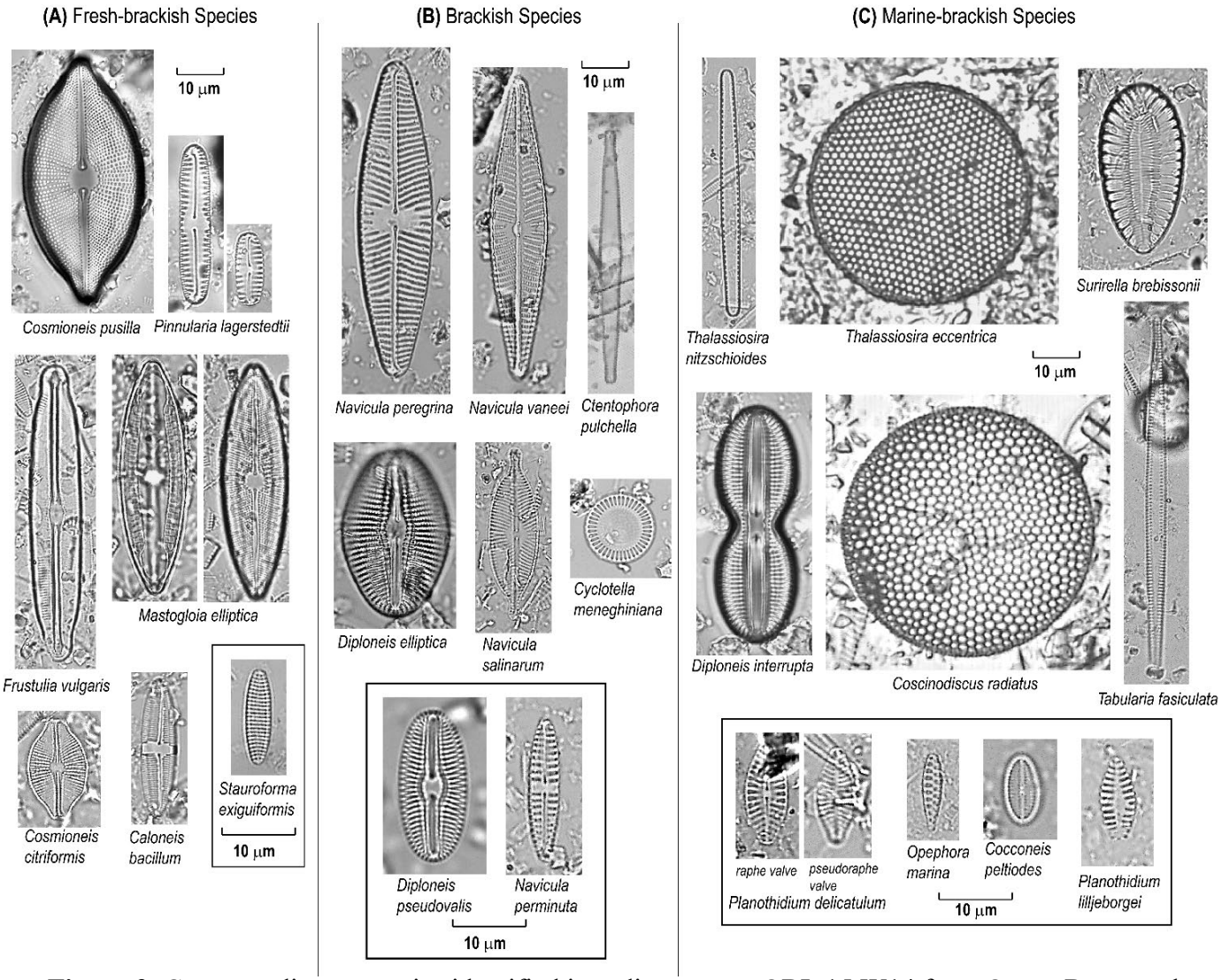

Figure 9. Common diatom species identified in sediment core OBL.15.W14 from Ocean Bay marsh, Sitkalidak Island, AK. Diatoms grouped by salinity preference and preferred tidal habitat.

REFERENCES

Atwater, B. F. (1987). Evidence for great Holocene earthquakes along the outer coast of Washington State. *Science*, *236*(4804), 942–944.

Blott, S. J., & Pye, K. (2001). GRADISTAT: a grain size distribution and statistics package for the analysis of unconsolidated sediments. *Earth Surface Processes and Landforms*, *26*(11), 1237–1248.

Briggs, R. W. (2006). Deformation and Slip Along the Sunda Megathrust in the Great 2005 Nias-Simeulue Earthquake. *Science*, *311*(5769), 1897–1901. https://doi.org/10.1126/science.1122602

Briggs, R. W., Engelhart, S. E., Nelson, A. R., Dura, T., Kemp, A. C., Haeussler, P. J., Corbett, D. R., Angster, S. J., & Bradley, L.-A. (2014). Uplift and subsidence reveal a nonpersistent megathrust rupture boundary (Sitkinak Island, Alaska): COSEISMIC LAND-LEVEL CHANGE, SITKINAK. *Geophysical Research Letters*, *41*(7), 2289–2296. https://doi.org/10.1002/2014GL059380

Carver, G., Gilpin, I. M., & Jacobson, M. L. (1992). Paleoseismicity of Kodiak Island, Alaska. *Jacobson, ML, Compiler, National Earthquake Hazards Reduction Program, Summaries of Technical Reports*, *33*, 92–258.

Carver, G., & Plafker, G. (2008). Paleoseismicity and neotectonics of the Aleutian subduction zone—An overview. *Washington DC American Geophysical Union Geophysical Monograph Series*, *179*, 43–63.

Carver, G., & Plafker, G. (2013). Paleoseismicity and Neotectonics of the Aleutian Subduction Zone-An Overview. In J. T. Freymueller, P. J. Haeussler, R. L. Wesson, & G. Ekström (Eds.), *Geophysical Monograph Series* (pp. 43–63). American Geophysical Union. https://doi.org/10.1029/179GM03

Cisternas, M., Garrett, E., Wesson, R., Dura, T., & Ely, L. L. (2017). Unusual geologic evidence of coeval seismic shaking and tsunamis shows variability in earthquake size and recurrence in the area of the giant 1960 Chile earthquake. *Marine Geology*, *385*, 101–113. https://doi.org/10.1016/j.margeo.2016.12.007

Dawson, A. G., & Shi, S. (2000). Tsunami deposits. *Pure and Applied Geophysics*, *157*(6), 875–897.

Dawson, A. G., & Stewart, I. (2007). Tsunami deposits in the geological record. *Sedimentary Geology*, *200*(3–4), 166–183. https://doi.org/10.1016/j.sedgeo.2007.01.002

Dura, T., Cisternas, M., Horton, B. P., Ely, L. L., Nelson, A. R., Wesson, R. L., & Pilarczyk, J. E. (2015). Coastal evidence for Holocene subduction-zone earthquakes and tsunamis in central Chile. *Quaternary Science Reviews*, *113*, 93–111. https://doi.org/10.1016/j.quascirev.2014.10.015

Dura, T., Engelhart, S. E., Vacchi, M., Horton, B. P., Kopp, R. E., Peltier, W. R., & Bradley, S. (2016). The Role of Holocene Relative Sea-Level Change in Preserving Records of Subduction Zone Earthquakes. *Current Climate Change Reports*, *2*(3), 86–100. https://doi.org/10.1007/s40641-016-0041-y

Dura, T., & Hemphill-Haley, E. (2020). Diatoms in tsunami deposits. In *Geological Records of Tsunamis and Other Extreme Waves* (pp. 291–322). Elsevier. https://doi.org/10.1016/B978-0-12-815686-5.00014-6

Dura, T., Hemphill-Haley, E., Sawai, Y., & Horton, B. P. (2016). The application of diatoms to reconstruct the history of subduction zone earthquakes and tsunamis. *Earth-Science Reviews*, *152*, 181–197. https://doi.org/10.1016/j.earscirev.2015.11.017

Dura, T., Horton, B. P., Cisternas, M., Ely, L. L., Hong, I., Nelson, A. R., Wesson, R. L., Pilarczyk, J. E., Parnell, A. C., & Nikitina, D. (2017). Subduction zone slip variability during the last millennium, south-central Chile. *Quaternary Science Reviews*, *175*, 112–137. https://doi.org/10.1016/j.quascirev.2017.08.023

Eckel, E. B. (1970). The Alaska Earthquake March 27, 1964: Lessons and Conclusions. *United States Department of the Interior*, *Geological Survey*, 67.

Engelhart, S., Witter, R., Briggs, R., Dura, T., Koehler, R., Vane, C., Nelson, A., Gelfenbaum, G., & Haeussler, P. (2018). *Historical and stratigraphic evidence for two ruptures of the Alaska-Aleutian megathrust in 1788* [Geophysical Research Abstracts].

Fournier, T. J., & Freymueller, J. T. (2007). Transition from locked to creeping subduction in the Shumagin region, Alaska. *Geophysical Research Letters*, *34*(6), L06303. https://doi.org/10.1029/2006GL029073

Garrett, E., Shennan, I., Woodroffe, S. A., Cisternas, M., Hocking, E. P., & Gulliver, P. (2015). Reconstructing paleoseismic deformation, 2: 1000 years of great earthquakes at Chucalén, south central Chile. *Quaternary Science Reviews*, *113*, 112–122. https://doi.org/10.1016/j.quascirev.2014.10.010

Gilpin, L. M. (1995). *Holocene paleoseismicity and coastal tectonics of the Kodiak Islands, Alaska*. University of California, Santa Cruz.

Hamilton, S., & Shennan, I. (2005a). Late Holocene great earthquakes and relative sea-level change at Kenai, southern Alaska. *Journal of Quaternary Science*, *20*(2), 95–111. https://doi.org/10.1002/jqs.903

Hamilton, S., & Shennan, I. (2005b). Late Holocene relative sea-level changes and the earthquake deformation cycle around upper Cook Inlet, Alaska. *Quaternary Science Reviews*, *24*(12–13), 1479–1498. https://doi.org/10.1016/j.quascirev.2004.11.003

Hamilton, S., Shennan, I., Combellick, R., Mulholland, J., & Noble, C. (2005). Evidence for two great earthquakes at Anchorage, Alaska and implications for multiple great earthquakes through the Holocene. *Quaternary Science Reviews*, *24*(18–19), 2050–2068. https://doi.org/10.1016/j.quascirev.2004.07.027

Hawkes, A. D., Horton, B. P., Nelson, A. R., & Hill, D. F. (2010). The application of intertidal foraminifera to reconstruct coastal subsidence during the giant Cascadia earthquake of AD 1700 in Oregon, USA. *Quaternary International*, *221*(1–2), 116–140.

Hemphill-Haley, E. (1996). Diatoms as an aid in identifying late-Holocene tsunami deposits. *The Holocene*, *6*(4), 439–448. https://doi.org/10.1177/095968369600600406

Hemphill-Haley, E., & Lewis, R. C. (2003). Diatom data from Bradley Lake, Oregon: Downcore analyses. *US Geological Survey Open-File Report*, *3*(190), 138.

Horton, B. P., Edwards, R. J., & Lloyd, J. M. (1999). UK intertidal foraminiferal distributions: Implications for sea-level studies. *Marine Micropaleontology*, *36*(4), 205–223.

Horton, B. P., Engelhart, S. E., Kemp, A. C., & Sawai, Y. (2013). 14.25 Microfossils in Tidal Settings as Indicators of Sea-Level Change, Paleoearthquakes, Tsunamis, and Tropical Cyclones. In *Treatise on Geomorphology* (pp. 292–314). Elsevier. https://doi.org/10.1016/B978-0-12-374739-6.00394-8

Horton, B. P., Milker, Y., Dura, T., Wang, K., Bridgeland, W. T., Brophy, L., Ewald, M., Khan, N. S., Engelhart, S. E., Nelson, A. R., & Witter, R. C. (2017). Microfossil measures of rapid sea-level rise: Timing of response of two microfossil groups to a sudden tidal-flooding experiment in Cascadia. *Geology*, *45*(6), 535–538. https://doi.org/10.1130/G38832.1

Horton, B. P., & Sawai, Y. (2010). Diatoms as indicators of former sea levels, earthquakes, tsunamis, and hurricanes. In J. P. Smol & E. F. Stoermer (Eds.), *The Diatoms* (2nd ed., pp. 357–372). Cambridge University Press. https://doi.org/10.1017/CBO9780511763175.020

Janigian, G. (2018). *A stratigraphic and microfossil record of coseismic land-level changes and tsunami deposits from Old Harbor, Central Kodiak Island, Alaska* [University of Rhode Island]. https://doi.org/10.23860/thesis-janigian-greta-2018

Jankaew, K., Atwater, B. F., Sawai, Y., Choowong, M., Charoentitirat, T., Martin, M. E., & Prendergast, A. (2008). Medieval forewarning of the 2004 Indian Ocean tsunami in Thailand. *Nature*, *455*(7217), 1228–1231. https://doi.org/10.1038/nature07373

Kachadoorian, R., & Plafker, G. (1967). *Effects of the Earthquake of March 27, 1964, on the Communities of Kodiak and Nearby Islands*. *Geological Survey*, 55.

Kelsey, H. M., Witter, R. C., Engelhart, S. E., Briggs, R., Nelson, A., Haeussler, P., & Corbett, D. R. (2015). Beach ridges as paleoseismic indicators of abrupt coastal subsidence during subduction zone earthquakes, and implications for Alaska-Aleutian subduction zone paleoseismology, southeast coast of the Kenai Peninsula, Alaska. *Quaternary Science Reviews*, *113*, 147–158. https://doi.org/10.1016/j.quascirev.2015.01.006

Kemp, A. C., Horton, B. P., Vane, C. H., Bernhardt, C. E., Corbett, D. R., Engelhart, S. E., Anisfeld, S. C., Parnell, A. C., & Cahill, N. (2013). Sea-level change during the last 2500 years in New Jersey, USA. *Quaternary Science Reviews*, *81*, 90–104.

Morton, R. A., Gelfenbaum, G., & Jaffe, B. E. (2007). Physical criteria for distinguishing sandy tsunami and storm deposits using modern examples. *Sedimentary Geology*, *200*(3–4), 184–207. https://doi.org/10.1016/j.sedgeo.2007.01.003

Mueller, C. S., Briggs, R. W., Wesson, R. L., & Petersen, M. D. (2015). Updating the USGS seismic hazard maps for Alaska. *Quaternary Science Reviews*, *113*, 39–47. https://doi.org/10.1016/j.quascirev.2014.10.006

Nelson, A. R., Briggs, R. W., Dura, T., Engelhart, S. E., Gelfenbaum, G., Bradley, L.-A., Forman, S. L., Vane, C. H., & Kelley, K. A. (2015). Tsunami recurrence in the eastern Alaska-Aleutian arc: A Holocene stratigraphic record from Chirikof Island, Alaska. *Geosphere*, *11*(4), 1172–1203. https://doi.org/10.1130/GES01108.1

Nelson, A. R., Hawkes, A. D., Sawai, Y., Engelhart, S. E., Witter, R., Grant-Walter, W. C., Bradley, L.-A., Dura, T., Cahill, N., & Horton, B. (2020). Identifying the greatest earthquakes of the past 2000 years at the Nehalem River Estuary, Northern Oregon Coast, USA. *OpenQuaternary.*, *6*(2), 1–30.

Nelson, A. R., Sawai, Y., Jennings, A. E., Bradley, L.-A., Gerson, L., Sherrod, B. L., Sabean, J., & Horton, B. P. (2008). Great-earthquake paleogeodesy and tsunamis of the past 2000 years at Alsea Bay, central Oregon coast, USA. *Quaternary Science Reviews*, *27*(7–8), 747–768.

Nelson, A. R., Shennan, I., & Long, A. J. (1996). Identifying coseismic subsidence in tidal-wetland stratigraphic sequences at the Cascadia subduction zone of western North America. *Journal of Geophysical Research: Solid Earth*, *101*(B3), 6115–6135. https://doi.org/10.1029/95JB01051

Plafker, G. (1965). Tectonic Deformation Associated with the 1964 Alaska Earthquake: The earthquake of 27 March 1964 resulted in observable crustal deformation of unprecedented areal extent. *Science*, *148*(3678), 1675–1687.

Plafker, G. (1969). Tectonics of the March 27th, 1964 Alaska earthquake. *United States Department of the Interior*, *543–I*, 74.

Plafker, G., & Kachadoorian, R. (1966). *Geologic Effects of the March 1964 Earthquake And Associated Seismic Sea Waves on Kodiak And Nearby Islands, Alaska*.

Rhodes, B., Tuttle, M., Horton, B., Doner, L., Kelsey, H., Nelson, A., & Cisternas, M. (2006). Paleotsunami research. *Eos, Transactions American Geophysical Union*, *87*(21), 205. https://doi.org/10.1029/2006EO210002

Ross, S. L., Jones, L. M., Miller, K. H., Porter, K. A., Wein, A., Wilson, R. I., Bahng, B., Barberopoulou, A., Borrero, J. C., & Brosnan, D. M. (2013). *SAFRR (Science Application for Risk Reduction) Tsunami Scenario—Executive Summary and Introduction: Chapter A in The SAFRR (Science Application for Risk Reduction) Tsunami Scenario*. US Geological Survey.

Sawai, Y. (2004). Transient Uplift After a 17th-Century Earthquake Along the Kuril Subduction Zone. *Science*, *306*(5703), 1918–1920. https://doi.org/10.1126/science.1104895

Sawai, Y., Namegaya, Y., Okamura, Y., Satake, K., & Shishikura, M. (2012). Challenges of anticipating the 2011 Tohoku earthquake and tsunami using coastal geology: ANTICIPATING THE 2011 TOHOKU EARTHQUAKE. *Geophysical Research Letters*, *39*(21), n/a-n/a. https://doi.org/10.1029/2012GL053692

Shanmugam, G. (2012). Process-sedimentological challenges in distinguishing paleo-tsunami deposits. *Natural Hazards*, *63*(1), 5–30. https://doi.org/10.1007/s11069-011-9766-z

Shennan, I., Barlow, N., Carver, G., Davies, F., Garrett, E., & Hocking, E. (2014). Great tsunamigenic earthquakes during the past 1000 yr on the Alaska megathrust. *Geology*, *42*(8), 687–690. https://doi.org/10.1130/G35797.1

Shennan, I., Brader, M. D., Barlow, N. L. M., Davies, F. P., Longley, C., & Tunstall, N. (2018). Late Holocene paleoseismology of Shuyak Island, Alaska. *Quaternary Science Reviews*, *201*, 380–395. https://doi.org/10.1016/j.quascirev.2018.10.028

Shennan, I., Bruhn, R., Barlow, N., Good, K., & Hocking, E. (2014). Late Holocene great earthquakes in the eastern part of the Aleutian megathrust. *Quaternary Science Reviews*, *84*, 86–97. https://doi.org/10.1016/j.quascirev.2013.11.010

Shennan, I., Bruhn, R., & Plafker, G. (2009). Multi-segment earthquakes and tsunami potential of the Aleutian megathrust. *Quaternary Science Reviews*, *28*(1–2), 7–13. https://doi.org/10.1016/j.quascirev.2008.09.016

Shennan, I., & Hamilton, S. (2006). Coseismic and pre-seismic subsidence associated with great earthquakes in Alaska. *Quaternary Science Reviews*, *25*(1–2), 1–8. https://doi.org/10.1016/j.quascirev.2005.09.002

Shennan, I., Scott, D. B., Rutherford, M., & Zong, Y. (1999). Microfossil analysis of sediments representing the 1964 earthquake, exposed at Girdwood Flats, Alaska, USA&. *Quaternary International*, 19.

Soloviev, S. L. (1990). Sanak-Kodiak tsunami of 1788. *Science of Tsunami Hazards*, *8*(1), 34–38.

Soria, J. L. A., Switzer, A. D., Pilarczyk, J. E., Siringan, F. P., Khan, N. S., & Fritz, H. M. (2017). Typhoon Haiyan overwash sediments from Leyte Gulf coastlines show local spatial variations with hybrid storm and tsunami signatures. *Sedimentary Geology*, *358*, 121–138. https://doi.org/10.1016/j.sedgeo.2017.06.006

Stein, S., & Okal, E. A. (2007). Ultralong Period Seismic Study of the December 2004 Indian Ocean Earthquake and Implications for Regional Tectonics and the Subduction Process. *Bulletin of the Seismological Society of America*, *97*(1A), S279–S295. https://doi.org/10.1785/0120050617

Stein, S., & Okal, E. A. (2011). The size of the 2011 Tohoku earthquake need not have been a surprise. *Eos, Transactions American Geophysical Union*, *92*(27), 227–228. https://doi.org/10.1029/2011EO270005

Suleimani, E. N., Nicolsky, D. J., & Koehler, R. D. (2017). *Updated Tsunami Inundation Maps of the Kodiak Area, Alaska*. State of Alaska, Department of Natural Resources, Division of Geological ….

Thatcher, W. (1984). The earthquake deformation cycle, recurrence, and the time-predictable model. *Journal of Geophysical Research: Solid Earth*, *89*(B7), 5674–5680. https://doi.org/10.1029/JB089iB07p05674

Troels-Smith, J. (1955). Karakterisering af løse jordarter. *Danmarks Geologiske Undersøgelse IV. Række*, *3*(10), 1–73.

von Huene, R., Miller, J. J., & Dartnell, P. (2016). A possible transoceanic tsunami directed toward the U.S. west coast from the Semidi segment, Alaska convergent margin: ALASKA TSUNAMI HAZARDS, SEMIDI SECTOR. *Geochemistry, Geophysics, Geosystems*, *17*(3), 645–659. https://doi.org/10.1002/2015GC006147

Vos', P. C., & de Wolf, H. (1993). *Diatoms as a tool for reconstructing sedimentary environments in coastal wetlands; methodological aspects*. 12.

Wang, P.-L., Engelhart, S. E., Wang, K., Hawkes, A. D., Horton, B. P., Nelson, A. R., & Witter, R. C. (2013). Heterogeneous rupture in the great Cascadia earthquake of 1700 inferred from coastal subsidence estimates: GREAT CASCADIA EARTHQUAKE OF 1700. *Journal of Geophysical Research: Solid Earth*, *118*(5), 2460–2473. https://doi.org/10.1002/jgrb.50101

Watcham, E. P., Shennan, I., & Barlow, N. L. M. (2013). Scale considerations in using diatoms as indicators of sea-level change: Lessons from Alaska. *Journal of Quaternary Science*, *28*(2), 165–179. https://doi.org/10.1002/jqs.2592

Wesson, R. L., Boyd, O. S., Mueller, C. S., Bufe, C. G., Frankel, A. D., & Petersen, M. D. (2007). Revision of time-independent probabilistic seismic hazard maps for Alaska. *US Geological Survey Open-File Report*, *1043*(2007), 33.

Witter, R. C., Briggs, R. W., Engelhart, S. E., Gelfenbaum, G., Koehler, R. D., & Barnhart, W. D. (2014). Little late Holocene strain accumulation and release on the Aleutian megathrust below the Shumagin Islands, Alaska. *Geophysical Research Letters*, *41*(7), 2359–2367. https://doi.org/10.1002/2014GL059393

Witter, R. C., Hemphill-Haley, E., Hart, R., & Gay, L. (2009). Tracking Prehistoric Cascadia Tsunami Deposits at Nestucca Bay, Oregon. *US Geological Survey, National Earthquake Hazards Reduction Program Final Technical Report 08HQGR0076*, *92*.

Witter, R. C., Kelsey, H. M., & Hemphill-Haley, E. (2003). Great Cascadia earthquakes and tsunamis of the past 6700 years, Coquille River estuary, southern coastal Oregon. *Geological Society of America Bulletin*, *115*(10), 1289. https://doi.org/10.1130/B25189.1

Wright, T. J. (2016). The earthquake deformation cycle. *Astronomy & Geophysics*, *57*(4), 4.20-4.26. https://doi.org/10.1093/astrogeo/atw148

Zong, Y., Shennan, I., Combellick, R. A., Hamilton, S. L., & Rutherford, M. M. (2003). Microfossil evidence for land movements associated with the AD 1964 Alaska earthquake. *The Holocene*, *13*(1), 7–20. https://doi.org/10.1191/0959683603hl590rp